JOURNAL OF GEOPHYSICAL RESEARCH, VOL. 103, NO. D18, PAGES 23,255–23,273, SEPTEMBER 27, 1998

A high-spectral resolution study of the near-infrared solar flux disposition in clear and overcast atmospheres

V. Ramaswamy and S. M. Freidenreich

NOAA Geophysical Fluid Dynamics Laboratory, Princeton University, Princeton, New Jersey

Abstract. The sensitivity of the near-infrared spectral atmospheric and surface fluxes to the vertical location of clouds is investigated, including a study of factors (drop-size distribution, drop optical depth, solar zenith angle, cloud geometrical thickness, atmospheric profiles) which govern this dependence. Because of the effects of the above-cloud, in-cloud and below-cloud water vapor the atmospheric absorbed flux in each spectral band depends critically on the cloud location, with a high cloud resulting in lesser absorption and greater reflection than a low one having the same drop optical depth. The difference between a high and a low cloud forcing of atmospheric absorption increases with drop optical depth. For any optical depth, clouds with larger drops cause a greater forcing of the spectral atmospheric absorption than those with smaller ones, so high clouds can even cause an increase rather than a decrease of the atmospheric absorption relative to clear skies. In contrast, the spectral and total surface fluxes are relatively insensitive to cloud vertical location. Instead, they are determined by the drop characteristics, notably drop optical depth. This near-invariance characteristic is attributable to the fact that most of the insolation reaching the surface is in the weak water vapor spectral absorption regions; here drops dominate the radiative interactions and thus there is little dependence on cloud height. In addition, the overlap of the drop spectral features with the moderate-to-strong vapor absorption bands ensures that insolation in these regimes fails to reach the surface no matter where the cloud is located; instead, these bands contribute the most to atmospheric absorption. The near-invariant behavior of the spectral and total surface flux holds separately for a wide variety of conditions studied. As a consequence, the difference in reflection, between two columns containing clouds with the same optical depth but located at different altitudes, is approximately balanced in magnitude by the difference in the atmospheric absorption; this holds for every spectral interval whether it be a weak, moderate, or strong vapor/drop absorption band. It also follows that the net fluxes at the top and surface of overcast atmospheres do not have a general, unambiguous relationship; this is in sharp contrast to a linear relation between them in clear skies. However, under certain overcast conditions (e.g., specific vertical location of clouds and solar zenith angle), a simple linear relationship is plausible.

1. Introduction

The interaction of solar radiation in cloudy atmospheres is an important component in the diabatic heating of the surface-atmosphere system and thus in the general circulation of the atmosphere. Several studies have estimated, using different types of radiative transfer models, the solar energy absorbed by clouds and atmosphere [e.g., *Liou*, 1976; *Stephens*, 1978; *Wiscombe et al.*, 1984; *Davies et al.*, 1984; *Slingo*, 1989; *Harshvardhan et al.*, 1987; *Schmetz*, 1993; *Ramaswamy and Freidenreich*, 1991, hereinafter referred to as RF91; *Chou et al.*, 1995; *Crisp*, 1997]. Over the years, the methods employed to compute the absorption have become increasingly refined and performed with increasing spectral resolution. Important points that have been unraveled by the above studies are the spectral features of the water vapor molecule across the near-infrared spectrum, its contrast with that for water in the condensed phase, and the importance of both in interactions with the incoming radiation that, in turn, governs the disposition within the atmosphere-surface system.

Here we inquire into the quantitative aspects of the interactions of the near-infrared solar radiation with water vapor and drops, with the primary objective being the sensitivity of the spectral and total fluxes absorbed in the atmosphere and surface to the vertical location of clouds. We examine the effects on this sensitivity due to considerations of different drop optical depths, drop-size distributions, atmospheric profiles, cloud vertical extents, and incident Sun angles. The investigations are performed by employing a highly accurate radiative transfer model which incorporates the detailed spectral features of water vapor and a rigorous multiple-scattering technique.

The present study extends the issues inquired into by earlier theoretical studies in two ways. First, the high spectral resolution computations performed here for an extensive range of parameter space provide a firm basis for gaging the relative quantitative roles of liquid water and water vapor in the spectral disposition of the near-infrared solar flux. In particular, this enables a detailed examination of the relationship between

Paper number 98JD02379.

the top-of-the-atmosphere (TOA), atmospheric absorbed, and surface spectral fluxes (Harshvardhan et al., unpublished data, 1997, hereinafter referred to as H97). Second, the spectrally integrated results serve as a rigorous means to examine the robustness of earlier ideas [e.g., *Chou*, 1989; *Schmetz*, 1993] concerning the overcast sky solar flux absorption in the atmosphere-surface system. The results here for plane-parallel clouds also provide a basis set for the calibration of solar radiative parameterizations typically employed in weather prediction and climate models. In addition, they are a reference point to study the departures in the solar flux disposition which occur for non-plane-parallel clouds.

2. Computational Model

The vertically inhomogeneous atmospheric model used for the calculations is the same as in RF91. It extends from 0 to 1013 mbar and consists of 51 layers, with the bottommost layer being 13 mbar and the rest 20 mbar thick. To represent the features of the in-cloud water vapor over each spectral interval with constant drop optical properties, we employ the "bin" algorithm described in RF91 and outlined below. The bin algorithm replaces the monochromatic vapor optical depth occurring in a cloud layer with a "representative" value. The monochromatic values at the discrete frequencies are obtained from considerations of the spectral line features of the molecule (i.e., line-by-line (LBL) method). The maximum and minimum vapor optical depth values that define the range of a bin are preset. The central value of the range spanned by a bin denotes the representative optical depth for all of the monochromatic values that fall within the range of that particular bin. This representative value is used in the multiple-scattering algorithm, together with the drop properties for the considered spectral interval, to obtain the cloud layer reflection and transmission for that bin. The binning process essentially reduces the number of monochromatic multiple-scattering calculations to be done for the cloud layer (RF91). The accuracy of the approximation is determined by the range spanned by the bins, with a greater accuracy resulting as the number of bins considered to cover the optical depth range of water vapor in any layer (range: 10^{-6}–10^{2}) is increased. For the present computations we employ the "$N = 90$" version of RF91. According to that study, the resulting accuracy is better than 0.1 and 1% in the total and spectral fluxes, respectively.

Only single cloud systems are considered. These may span multiple but contiguous model layers. The attenuation of the radiation stream emerging from the prescribed cloud layers is solved for in the usual LBL manner (i.e., without any "binning" approximation (RF91)) as it progresses through the layers containing water vapor to either the top or the bottom of the atmosphere. For clear-sky instances the LBL solution is used directly, that is, binning is unnecessary (see RF91).

While the line-by-line portion of the algorithm considers the individual spectral lines of the water vapor molecule, the doubling-adding method, a variant of that described by *Hunt and Grant* [1969; cf. RF91], treats the multiple-scattering accurately. Only water vapor and water drops are considered in this study. We employ 32 streams for the computations (RF91). The near-infrared solar spectral flux is the same as in RF91 with the total value in the 0–18000 cm^{-1} region (S_0) being 966 W/m^2 for overhead Sun conditions. We use the Air Force Geophysics Laboratory AFGL 1982 [*Rothman et al.*, 1983] line parameter catalog (tests using the AFGL 1992 catalog show insignificant differences in water vapor absorption across the near-infrared spectrum). To keep the focus on water vapor and drops, absorption by other gases and molecular scattering are ignored.

Clouds are assumed to be plane parallel and horizontally homogeneous. Cloud drop-size distributions and their single-scattering parameters follow either the CS or the CL cloud drop-size distributions [*Fouquart et al.*, 1991]; these were recommended as typical water cloud drop distributions in an international solar radiation intercomparison project. Unless otherwise stated, we analyze the results using the following parameters as the nominal ones: model layer CS clouds at three different altitudes, namely, 180–200 mbar (high), 500–600 mbar (middle), and 800–900 mbar (low); drop optical depths (τ_{drop}, the drop extinction optical depth at a wavelength of 0.55 μm) of 1, 10, and 100; near-overhead Sun conditions (zenith angle of 3°); and midlatitude summer (MLS) atmospheric profile [*McClatchey et al.*, 1972]. Additional calculations are performed for the following cases: 20 mbar thick CS clouds placed at different altitudes; other solar zenith angles; CS clouds with different geometrical thicknesses; other atmospheric profiles; other optical depths (τ_{drop} = 2, 3, 5, 7, 15, 20, 35, and 50) for both CS and CL clouds at high, middle, and low altitudes. Given the effective radii (5.25 μm for CS and 31 μm for CL), the optical depth range studied implies a range in liquid water path (LWP) of ~3–333 g/m^2 for CS and ~20–2000 g/m^2 for CL clouds.

All calculations consider a zero surface albedo in order to avoid the complexity of effects due to multiple scattering between surface and clouds. The cloud layers contain vapor corresponding to saturation conditions. To delineate the effect of vapor inside clouds, we also compute the fluxes for the corresponding "dropless" condition wherein there are no drops but the water vapor amount in the cloud layer is held at the appropriate saturation value. This is distinct from the "clear-sky" calculation where water vapor amount is not present at saturation values in any layer.

We restrict the study to considerations of drop-size distributions that are typical of water clouds. The presence of a CS or a CL water drop distribution at high altitudes may not be a realistic representation of typical condensate distributions there. However, recalling that the focus here is the sensitivity to height location, and in order not to confuse with the issue of the sensitivity to particle shape which is not the intent of this study, we consider only these two distributions. Figure 1 illustrates the spectral solar irradiance, column optical depth of water vapor in the MLS atmosphere (whose range extends to values $>10^3$), and the extinction coefficient, single-scattering coalbedo, and asymmetry factor of the two drop-size distributions. In contrast to drop extinction and asymmetry factor, both drop and water vapor absorption have distinct spectral variations, with water vapor having a much finer spectral dependence [see also *Davies et al.*, 1984; *Ramaswamy and Freidenreich*, 1992, hereinafter referred to as RF92). A significant atmospheric absorption is suggested by the overlap seen of spectral regions associated with both substantial irradiance and moderate-to-strong vapor and drop absorption.

3. Total Near-IR Flux Disposition

We designate the total flux reflected at the top-of-the-atmosphere (TOA) by $S^{\uparrow}_{TOA}$, that absorbed in the atmosphere by S^{abs}_{atm} and that reaching the surface by $S^{\downarrow}_{sfc}$. In addition, we

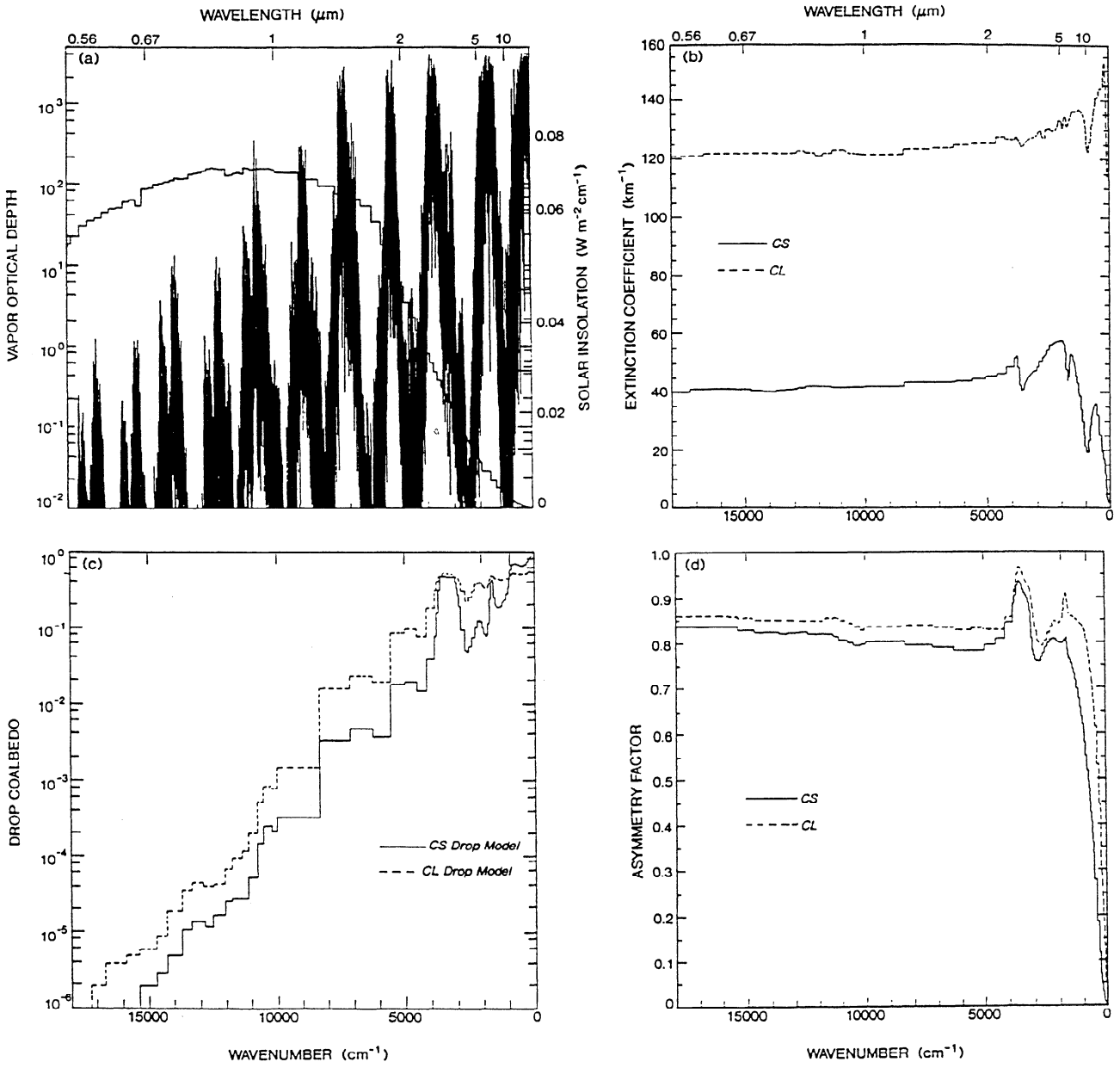

Figure 1. (a) Atmospheric vapor optical depth and the solar spectral irradiance (thin, solid curve) over the 0–18000 cm^{-1} near-infrared region. (b) Extinction coefficient, (c) single-scattering albedo, and (d) asymmetry factor of the CS and CL drop models. The wavelength scale is also indicated in brief.

use S^{abs}_{abcld}, S^{abs}_{cld}, and S^{abs}_{blcld} to denote the fluxes absorbed above, in, and below cloud, respectively.

Figure 2a shows, for the MLS sky, the percent of near-infrared incident flux reflected at TOA by high, middle, and low CS clouds as a function of τ_{drop}. Figures 2b and 2c show the flux absorbed in the atmosphere and that reaching the surface, along with the appropriate clear-sky values.

The reflected flux follows an expected pattern [e.g., *Liou*, 1976; *Stephens*, 1978] of a monotonic increase with optical depth for all three cloud levels but with a difference in the magnitudes for the three different cloud altitudes. The largest flux arises in the high-cloud case since, then, the cloud particles interact with the radiation before it can interact with vapor. Lower down, less solar energy is available for reflection by drops as water vapor above cloud attenuates the radiation.

The flux absorbed in an atmosphere with clouds at any level is, in general, not constant with optical depth nor is it the same for clouds at different altitudes. In comparison with the low cloud, the high cloud's greater reflection is accompanied by a lesser atmospheric absorption. In the low-cloud case, the water vapor above the cloud absorbs a substantial amount of radiation before it can impinge on the cloud [*Davies et al.*, 1984; RF91]. Compared to the clear-sky case with water vapor only, the high cloud causes the atmosphere to absorb less radiation, while the middle and low clouds absorb more. The absorbed flux increases with optical depth for the low cloud, while for the high cloud, there is a decrease with τ_{drop} up to ~10 after which there is a slight increase. The middle-cloud case exhibits relatively less variation with τ_{drop}. In general, with an increase in drop extinction optical depth, there is an increase in both the

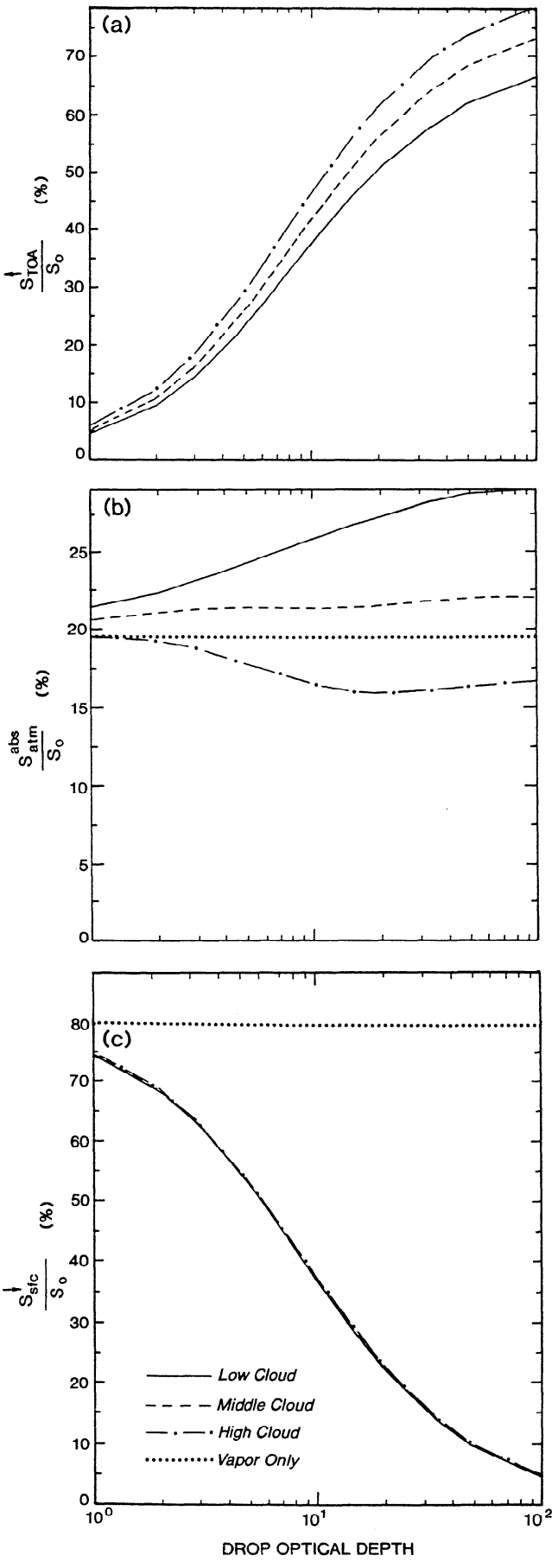

drop scattering and the absorption optical depths. For the high cloud, the net effect is a decrease in the atmospheric absorption with τ_{drop} owing to increased reflection outweighing the increased drop absorption. However, for $\tau_{drop} > 20$, the rate of increase of reflection is reduced, and there is an increase in the atmospheric absorption. For the low cloud the larger in-cloud vapor amount contributes to a greater layer single-scattering coalbedo compared to the high-cloud case. This, together with a relatively lesser rate of increase of reflection with optical depth (Figure 2a), contributes to a greater increase in atmospheric absorption with τ_{drop} (~1–60) than for the high cloud. For the middle cloud the increase of cloud absorption with drop optical depth is nearly offset by the increased reflection such that atmospheric absorption changes only slightly with τ_{drop}.

The flux at the surface varies in a monotonic fashion with τ_{drop} [see *Stephens*, 1978], decreasing with increasing optical thickness (Figure 2c). The flux differs markedly from that in clear skies even at the smallest optical depth considered. However, the most remarkable feature in this plot is the near constancy of the surface flux for clouds with the same τ_{drop} but located at different levels in the atmosphere, a feature pointed out earlier [e.g., *Chou*, 1989; *Schmetz*, 1993]. Figure 2 suggests that for any τ_{drop} the TOA reflected and surface fluxes cannot be related without additional knowledge about the location of the cloud.

The fluxes absorbed in the atmosphere are subdivided into that absorbed above, in, and below cloud in Figures 3a, 3b, and 3c. In each panel the values for corresponding dropless conditions (referred to the same cloud layers) are also indicated. The flux absorbed above the cloud (Figure 3a) shows only a slight increase with drop optical depth, indicating that most of the absorption takes place in the downward propagation of the direct beam. The absorption is greater when the cloudtop is lower because of the longer water vapor optical path then encountered by the reflected beam.

The flux absorbed within cloud increases with drop optical depth and is substantially enhanced with respect to the corresponding dropless condition (Figure 3b). At large optical depths ($\tau_{drop} > 50$) the high cloud absorbs more radiation than the middle and low clouds, quite the opposite of the features at smaller optical depths. For $\tau_{drop} < 50$, the middle cloud absorbs the most radiation and the high cloud the least. These features arise because the magnitude of cloud absorption, for a specific drop optical depth, is intimately related to how much radiation is absorbed by the water vapor above the cloud and to the amount of water vapor inside the cloud. In the case of the low cloud, there is more absorption by the above-cloud vapor, thus diminishing the ability of the cloud to absorb radiation relative to the middle cloud. Relative to the high cloud, the lower clouds have more water vapor, thus leading to a greater absorption at small drop optical depths. At large τ_{drop} values the drop effects dominate relative to vapor. However, because of the damping effect by the above-cloud vapor which depletes the beam in the spectral regions over which drops can

Figure 2. Fraction of the total incident near-infrared flux (966 W/m^2) which is (a) reflected, (b) absorbed in the atmosphere, and (c) transmitted to the surface as a function of drop optical depth for high (180–200 mbar), middle (500–600 mbar), and low (800–900 mbar) CS clouds in a midlatitude summer (MLS) atmosphere. Solar zenith angle is 3°. Also indicated in Figure 2b and 2c are the clear-sky values.

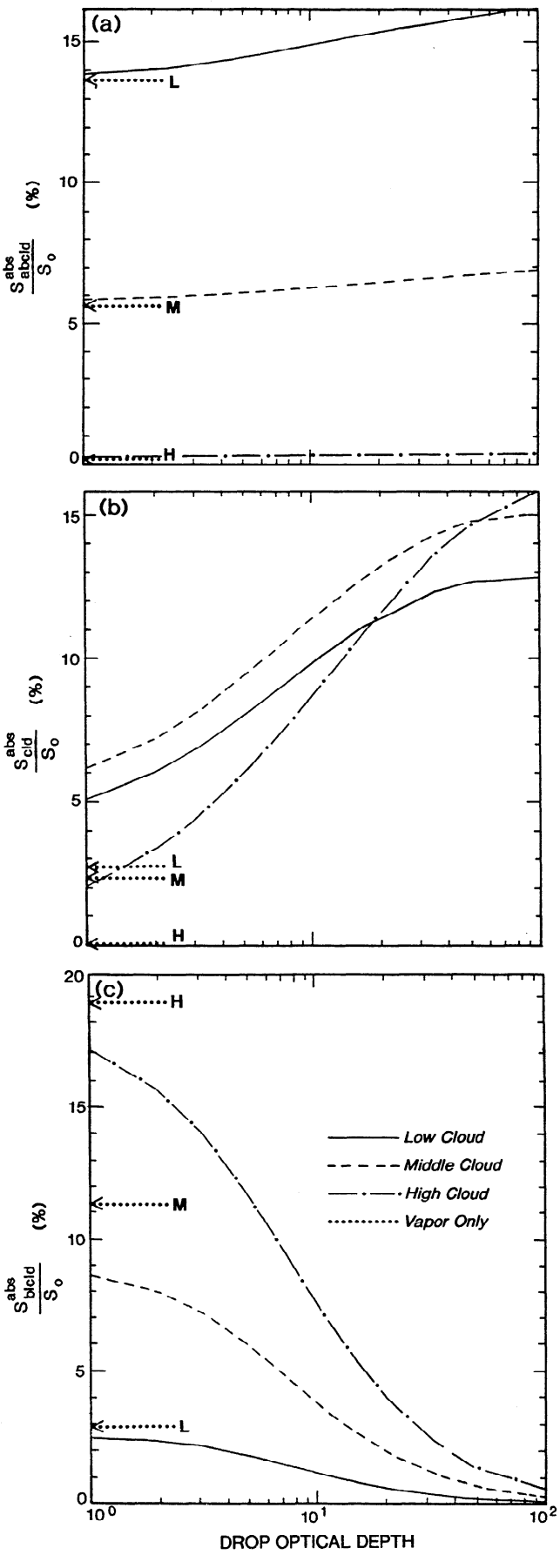

be effective in absorption, the low cloud cannot yield so large an absorption as the high cloud layer at large τ_{drop} values. The dominance of the drops' effect over vapor also leads to a more rapid increase of the absorption with τ_{drop} for the high-cloud case. The modulating effect of the above-cloud vapor absorption is also seen by comparing the cloud-absorbed flux with the atmospheric absorbed flux (Figure 2b). Even though the middle-cloud absorption exceeds that of the low cloud, the atmospheric absorption is more in the low-cloud case owing to the considerable contribution by the above-cloud vapor absorption. Further, even though the high-cloud layer absorption exceeds the middle and low clouds at large optical depths, the total atmospheric absorption is the least for the high cloud (making it even less than in clear sky (Figure 2b)), thus reiterating the significance of the above-cloud water vapor.

The flux absorbed below clouds (Figure 3c) decreases with optical depth, with the most absorption occurring for the high cloud, since the path length becomes the longest for this case relative to the other two clouds. Note that the magnitude of absorption above or below clouds can range to ~17% indicating that the distribution of absorption in cloudy atmospheres has to account for the noncloud layer atmospheric component as well. The difference from dropless sky absorption is greatest for high clouds with large τ_{drop} since then the below-cloud water vapor absorption is less owing to the dominance of the interactions by the drops. In general, with increasing τ_{drop} the fluxes absorbed in the atmosphere begin to depart substantially from the dropless sky absorption.

To capture the variation of the absorption with cloud location in the entire atmosphere and simultaneously at several drop optical depths, we next consider 20 mbar CS clouds placed successively at 40 mbar height intervals. The absorbed fluxes in the atmosphere plus surface system (S^{net}_{TOA}), atmosphere only, and cloud only are shown in Figures 4a, 4b, and 4c, respectively. The rate of increase of the atmosphere plus surface absorption with decreasing cloud altitude due to the above-cloud vapor absorption is more so at the lower cloud locations. Increases in τ_{drop} result in a progressive enhancement of the flux difference between upper troposphere and lower cloud locations, consistent with Figure 2a. The fact that for small τ_{drop} the atmosphere plus surface absorption is the same no matter where the cloud is located does not necessarily mean that the atmosphere and surface absorption individually are invariant. In fact, from Figure 2c, this property holds only for the surface flux.

The flux absorbed within clouds (Figure 4c) increases slightly at first with decreasing cloud height owing to increasing in-cloud vapor content but eventually decreases as vapor above cloud depletes radiation that the cloud layer could have absorbed, consistent with Figure 3b. At large optical depths the in-cloud vapor effect is small relative to drops, resulting in a monotonic decrease of absorption with decreasing cloud

Figure 3. Fraction of the total incident near-infrared insolation absorbed (a) above-, (b) in-, and (c) below-cloud layers as a function of optical depth. The high, middle, and low clouds and the conditions considered are the same as in Figure 2. Arrows denote the corresponding absorption computed under the hypothetical assumption of "dropless" skies (but with saturated water vapor amounts in the concerned layers) for each of the cloud locations. L, M, and H refer to low, middle, and high dropless cases.

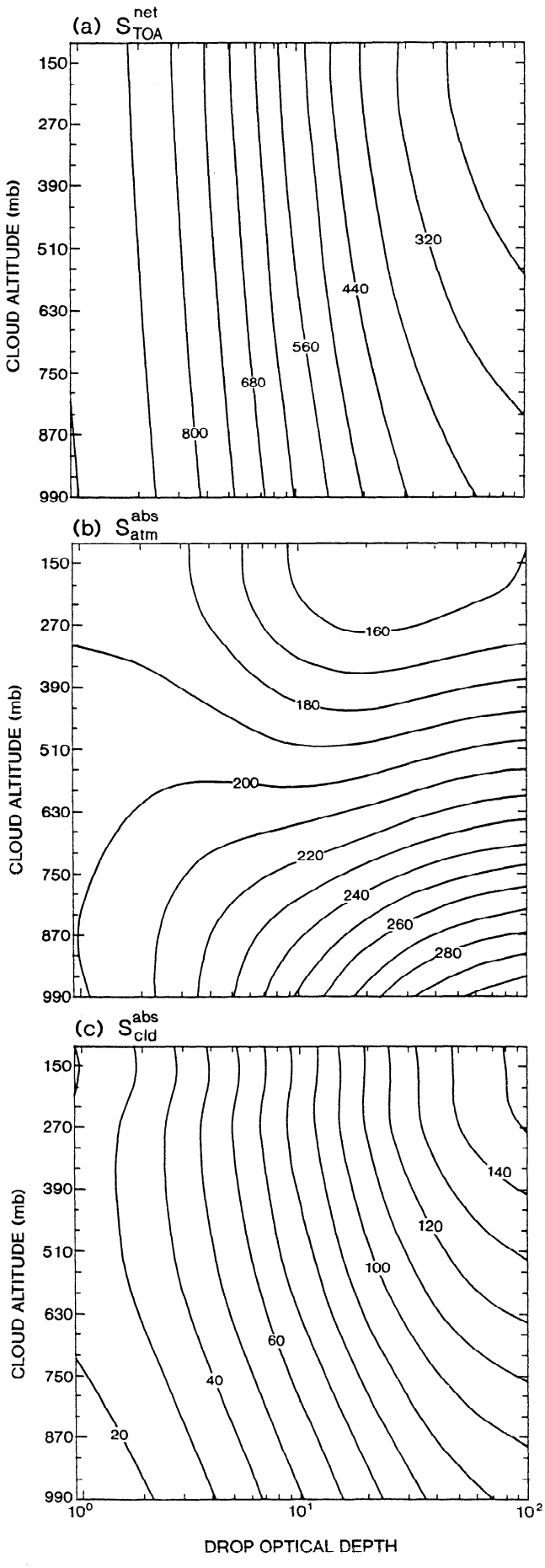

Table 1. Solar Flux Absorbed (W/m^2) in the Cloud Layer Under Three Different Assumptions

Cloud Location	τ_{drop}	Drop Only	Drop + in-Cloud Vapor	Full
High	1	14.9	20.6	19.7
Middle	1	14.9	102.5	59.3
Low	1	14.9	143.5	49.2
High	10	80.5	84.9	83.4
Middle	10	80.5	151.5	109.5
Low	10	80.5	195.2	94.7
High	100	153.1	154.3	152.7
Middle	100	153.1	183.4	145.2
Low	100	153.1	206.1	123.3

Low (800–900 mbar), middle (500–600 mbar), and high (180–200 mbar) CS type clouds are considered in a MLS atmosphere. Drop optical depths (τ_{drop}) considered are 1, 10, and 100. Solar zenith angle is 3°. The "drop-only" case is with the complete absence of water vapor everywhere, the "drop plus in-cloud vapor" has vapor only in the cloud layer, while the "full" case is the nominal one with vapor present above, in, and below the cloud layer (see section 3).

height, in line with the damping by the above-cloud vapor. The altitudinal variation is enhanced at lower cloud locations, more so at larger τ_{drop}.

The distinct variation of the absorbed flux in the atmosphere (Figure 4b) reinforces the inference that both optical depth and cloud location are significant. The pattern of variation from top to bottom is unlike that for the atmosphere plus surface and cloud layer absorption, whether seen in terms of cloud location or τ_{drop}. There is, however, a monotonic increase in absorption with decreasing cloudtop owing to above- and in-cloud vapor effects, thus adding a generality to the results in Figure 2b. Above 500 mbar an increase in τ_{drop} leads, first, to a decrease in absorption owing to increased cloud reflection. However, at large τ_{drop}, drop absorption increases (see Figure 4c). In contrast, for low clouds ($P > 500$ mbar), the absorption increases monotonically with τ_{drop}. From Figure 4b there is no unique variation of the atmospheric absorption with height for any drop optical depth, nor is there an unambiguous relation between the parameters considered in the three panels. This implies that the net flux at TOA cannot yield meaningful information about atmosphcric absorption without knowledge or assumption of cloud height (also, implicitly, vapor profile) and optical depth.

The effect of water vapor is highlighted by conducting a separate sensitivity study (Table 1). We consider the 180–200, 500–600, and 800–900 mbar clouds with τ_{drop} of 1, 10, and 100. We make three distinct assumptions: drops only (i.e., no vapor in the atmosphere), drops plus in-cloud vapor at saturation value (i.e., no vapor elsewhere in the atmosphere), and the "full" case (i.e., drop plus vapor in the entire atmosphere). The drop plus in-cloud vapor case absorbs the most radiation, especially low clouds which contain the most in-cloud vapor and thus the greatest single-scattering layer coalbedo. The in-cloud vapor's enhancement is less effective for optically thicker clouds when drop absorption dominates. There is a lesser ab-

Figure 4. Flux absorbed (W/m^2) by (a) surface plus atmosphere, (b) atmosphere, and (c) within clouds, as a function of drop optical depth, for 20 mbar thick CS clouds located at different pressure altitudes in the MLS atmosphere. Solar zenith angle is 3°.

sorption in the full case owing to the attenuation by the above-cloud vapor, with the highest cloud case exhibiting the least such reduction.

4. Spectral Flux Disposition

We next discuss the spectral aspects by summing fluxes over definite intervals or bands. $\sigma_{TOA}^{\downarrow-\uparrow}$, σ_{atm}^{abs}, and $\sigma_{sfc}^{\downarrow}$ denote the incident, reflected, atmospheric absorbed, and surface fluxes, respectively, over the considered intervals. Unless otherwise stated, the intervals are 100 cm^{-1} wide.

Figure 5 illustrates the spectral fraction of the total TOA incident flux and the corresponding fractions absorbed by the atmosphere and reaching the surface in a MLS profile with vapor only. Below 8000 cm^{-1} there are several bands (e.g., ~3700, 5400, 7300 cm^{-1}) wherein the entire incident radiation is absorbed. Beyond 8000 cm^{-1} the bands are unsaturated with respect to vapor absorption. There also exist bands wherein all of the TOA incident radiation reaches the surface with negligible attenuation in the atmosphere, for example, ~2500, 4500, 6300, 8000, 9600, and 11,500 cm^{-1}. The main contribution to the total surface flux arises from the spectral regime >6000 cm^{-1} (cf. RF91), whereas for atmospheric absorption, it arises from regimes below ~10,500 cm^{-1} [cf. *Ramaswamy and Li*, 1996].

We consider next high, middle, and low CS cloud cases with τ_{drop} of 1, 10, and 100. The reflected, atmospheric absorbed and surface flux spectral fractions are illustrated in Figure 6. The clear-sky results are reproduced in column 1 of Figure 6.

The fine spectral variation of the overcast sky fluxes is seen to depend crucially on the absorption features of water vapor; for example, for the low cloud case, when a longer vapor path length is traversed by the photons, there results more absorption and less reflection compared to the high cloud, with the spectral reflection generally negatively correlated with the absorbed flux. The absorption for $\tau_{drop} = 1$ is nearly similar to the "clear" sky results, but the surface flux is distinctly less. The spectral variation in reflection is less for the high cloud since it is governed more by the relatively broad spectral variation of the drop properties (single-scattering coalbedo (Figure 1c); this becomes even more pronounced at large optical depths ($\tau_{drop} = 100$) when the spectral variation of the atmospheric absorbed and surface fluxes is also considerably suppressed. These spectral features, arising due to the combination of cloud location and the role of water vapor, could be of considerable utility for remote sensing strategies employing high-spectral resolution (H97).

The most striking feature of Figure 6 is the near-invariance of the spectral surface flux with respect to cloud height, irrespective of the drop optical depth. This makes it clear that the feature seen in Figure 2c for the total near-infrared flux does not arise due to offsets of contributions from different portions of the spectrum. The compensatory effect between reflected and atmospheric absorbed fluxes is such that the surface spectral flux for the three cloud locations remains identical throughout the spectrum. However, the cloudy sky surface flux does differ from the clear-sky value, especially in the weakly absorbing water vapor regions (e.g., 4500, 6300, 8000, 9600 cm^{-1}).

The spectrally distinct signature cast by vapor, both in clear and in cloudy sky absorption (Figures 5 and 6), makes it apparent that the near-infrared spectrum cannot be thought of as composed of either totally absorbing or nonabsorbing spectral

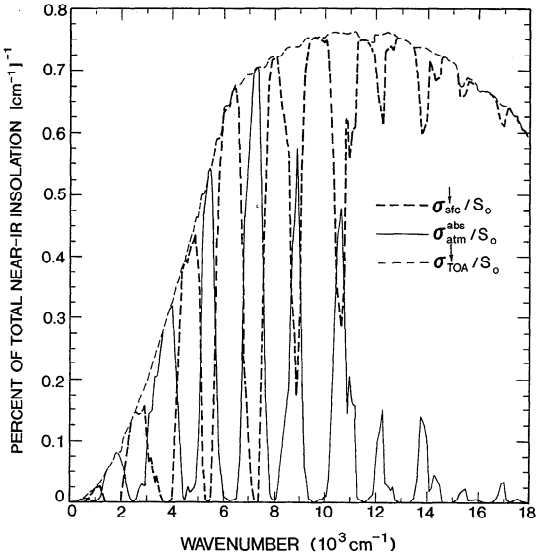

Figure 5. Spectral distribution of the near-infrared flux incident at the top-of-the-atmosphere ($\sigma_{TOA}^{\downarrow}$), that absorbed in the atmosphere (σ_{atm}^{abs}) and that reaching the surface ($\sigma_{sfc}^{\downarrow}$), expressed as a fraction of the total TOA insolation (S_0), in the MLS atmosphere containing only water vapor. Solar zenith angle is 3°.

regions. The varying strengths of reflection and absorption enhancements in different spectral intervals due to clouds are summarized in the form of a scatterplot (Figure 7). Here the change (i.e., cloud minus clear sky) in the spectral TOA albedo (change in spectral reflected flux divided by the near-infrared insolation) versus that in absorptivity (change in spectral absorbed flux divided by the near-infrared insolation) is plotted for the high (Figure 7a) and low (Figure 7b) cloud cases ($\tau_{drop} = 10$). For high cloud, several spectral intervals exhibit a high reflection but very little change in absorption; this is due to either the decrease in water vapor absorption below cloud (relative to clear sky) being compensated by the drop absorption or due to very weak absorption by both drops and vapor; in some other intervals, there is a net reduction of atmospheric absorption. There are also intervals where absorption exceeds that in "clear" sky and where the reflection can be weak or strong. The low-cloud case is significantly different. All intervals exhibit greater absorption than the clear sky whether or not the reflection is enhanced substantially. From Figure 7 it is difficult to argue for a general correlation between absorption and reflection across the spectrum; that is, different spectral intervals can yield unique enhancements with respect to clear sky. Cloud altitude is also a major factor. Note that the richness of the spectral enhancements for different clouds is not made evident by Figure 2b.

The role of the spectrally dependent effects due to vapor is examined by focusing on the low cloud case, which yields a greater role for the above- and in-cloud vapor relative to the high-cloud case. Figure 8 shows the atmospheric absorbed and surface fluxes, with drops only, with drops and vapor above- and below-cloud only, and the full atmosphere case ($\tau_{drop} = 10$). The drop-only case represents limiting conditions, i.e., extremely dry atmospheres; in this limit, the spectral surface flux would be the same irrespective of cloud location. The drop-only case yields much less spectral absorption than the full atmosphere case, with little radiation absorbed beyond

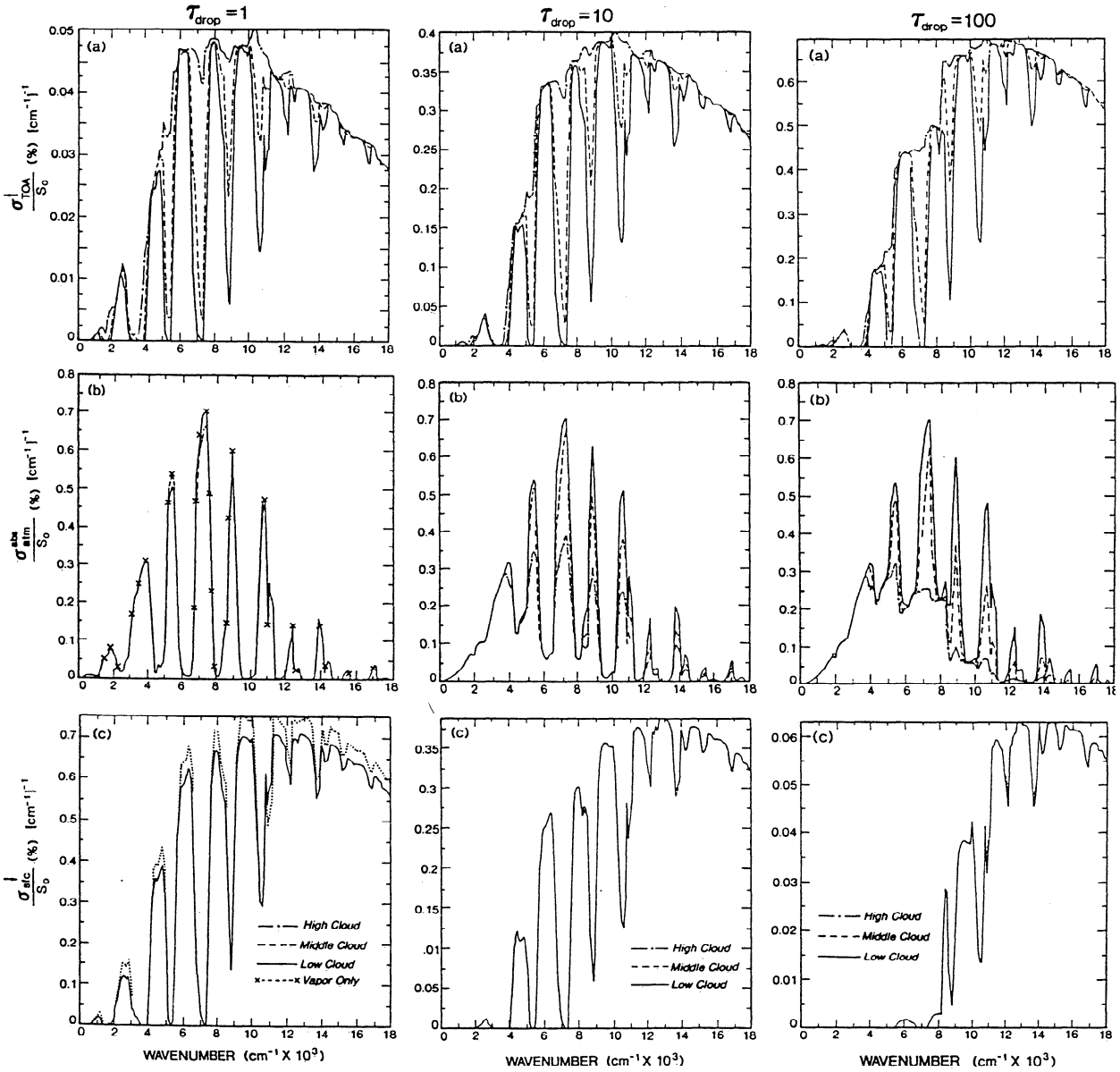

Figure 6. Spectral distribution of the fraction of the total near-infrared insolation (S_0) which is reflected (top panels, $\sigma^{\uparrow}_{TOA}$), absorbed in the atmosphere (middle panels, σ^{abs}_{atm}), and transmitted to the surface (bottom panels, $\sigma^{\downarrow}_{sfc}$) due to CS clouds at high, middle, and low locations. The three columns correspond to drop optical depths of (a) 1, (b) 10, and (c) 100, respectively. Solar zenith angle is 3°. Column 1 also displays the clear-sky values reproduced from Figure 5.

8000 cm^{-1}. Compared to drops only, vapor adds substantially to the absorption between 3000 and 14000 cm^{-1}. This is made up of largely the above-cloud vapor absorption [cf. *Davies et al.*, 1984], with the vapor inside cloud adding some more, notably around 9000, 11,000, and 14,000 cm^{-1} where drop absorption is weak. Relative to the drop-only case, the vapor reduces the surface flux, with the above-cloud vapor's contribution exceeding considerably that of the in-cloud vapor.

5. Analyses of Spectral Fluxes

We analyze next the relative contributions of the spectral atmospheric absorbed and surface transmitted fluxes from different portions of the spectrum. Bearing in mind the nonmonotonic variation of the fluxes across the spectrum (Figures 1, 5, and 6), we perform the analysis not in terms of wavenumber space but rather in terms of increasing vapor optical depth. We perform a sorting of the cloudy sky flux results in terms of the total atmospheric vapor optical depth arranged into five categories or bins (note that this binning is quite different from that described in section 2 for the radiative transfer computations): $<10^{-3}$ (very weak), 10^{-3}–10^{-1} (weak), 10^{-1}–10^{0} (moderate), 10^{0}–10^{1} (strong), and $>10^{1}$ (very strong). First, the "effective" atmospheric water vapor optical depth over each wavenumber is obtained from the clear-sky LBL transmission averages as follows:

$$\tau = -\mu_0[\ln(\sigma^{\downarrow}_{sfc}/\sigma^{\downarrow}_{TOA})]$$

where the sigmas here denote sums over 1 cm^{-1}, and μ_0 is the cosine of the solar zenith angle, with the results for the 3°

incidence used here as an example. Then, the atmospheric-absorbed and surface-transmitted fluxes in the overcast sky cases obtained for each of the 1 cm^{-1} intervals are segregated into the appropriate water vapor optical depth category. This procedure essentially pools together spectral regions that may be widely separated in wavenumber space but that have similar atmospheric vapor optical depths. The sum of the 1 cm^{-1} absorbed flux in each of the five categories is divided by the total absorbed flux to obtain their fractional contributions to the atmospheric absorption. A similar procedure is performed to obtain the fractional contributions to the total transmission.

Figure 9 (left) shows the contribution (ϕ_{abs}) to the atmospheric absorption from each of the five bins for the high-, middle-, and low-cloud cases, with the three panels denoting τ_{drop} = 1, 10, and 100. The clear-sky result is also shown in Figure 9a. While there is generally an increase of the relative contribution with increasing vapor optical depth category, the very strong category contributes less than the strong one owing, in part, to some 1 cm^{-1} intervals being associated with relatively less irradiance. For any τ_{drop} the relative contributions follow almost the same pattern for all cloud levels. For clear sky the absorption contributions are mainly from the moderate and the two stronger categories, while at large τ_{drop}, even the two weak categories can contribute significantly.

The corresponding result for the surface flux transmission (ϕ_{sfc} in right panels of Figure 9) reveals that the leading contributions (>85%) for both clear-sky and overcast sky instances arise mainly from the two weakly absorbing categories (vapor optical depths <0.1), in contrast to that seen for absorption. The pattern of relative contributions is nearly similar for all cloud locations and drop optical depths. Thus whether examined in spectral space (Figure 6c) or in terms of the grouping seen in Figure 9, the near-infrared constancy of the surface flux with respect to cloud placement is due to radiation

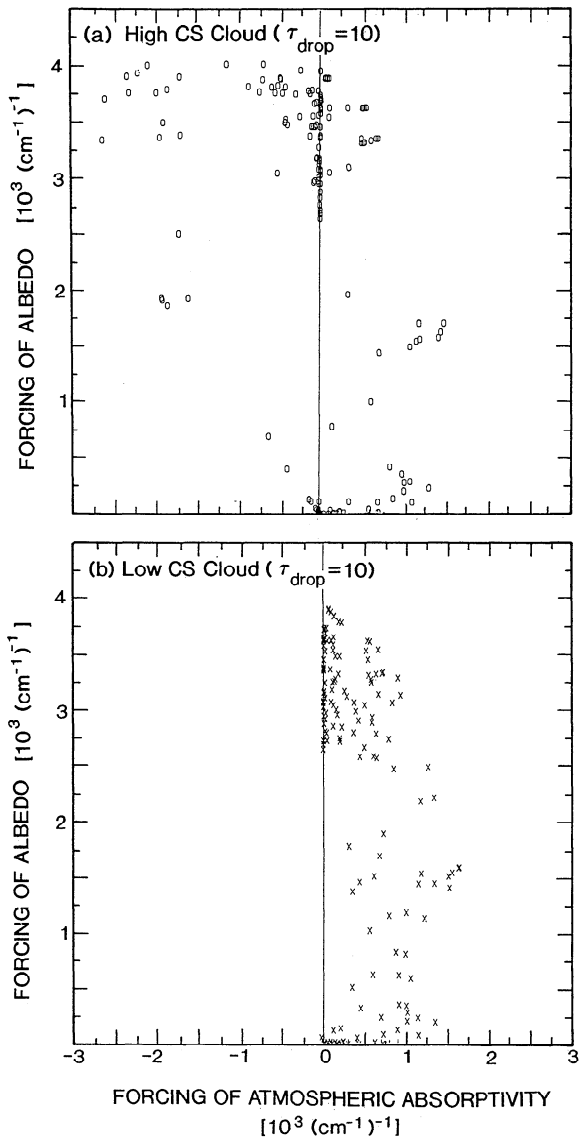

Figure 7. Scatterplot of the effect in different 100 cm^{-1} intervals of the enhancement (over clear sky) of the albedo versus the enhancement of the atmospheric absorption in the case of a (a) high and (b) low CS cloud. Values representing each spectral interval are expressed as a fraction of the total near-infrared TOA insolation. Solar zenith angle is 3°.

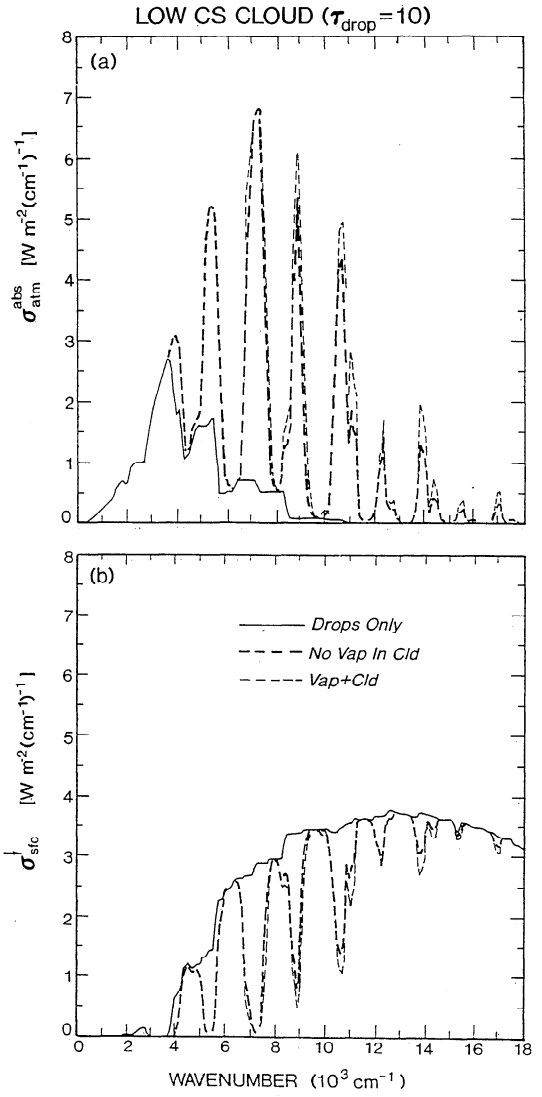

Figure 8. Spectral distribution of the flux (a) absorbed in the atmosphere and (b) reaching the surface in the case of a CS cloud under different assumptions. Solid line considers no vapor anywhere in the atmosphere; long-dashed line considers vapor everywhere except in the cloud; and short-dashed line considers the full case. Solar zenith angle is 3°.

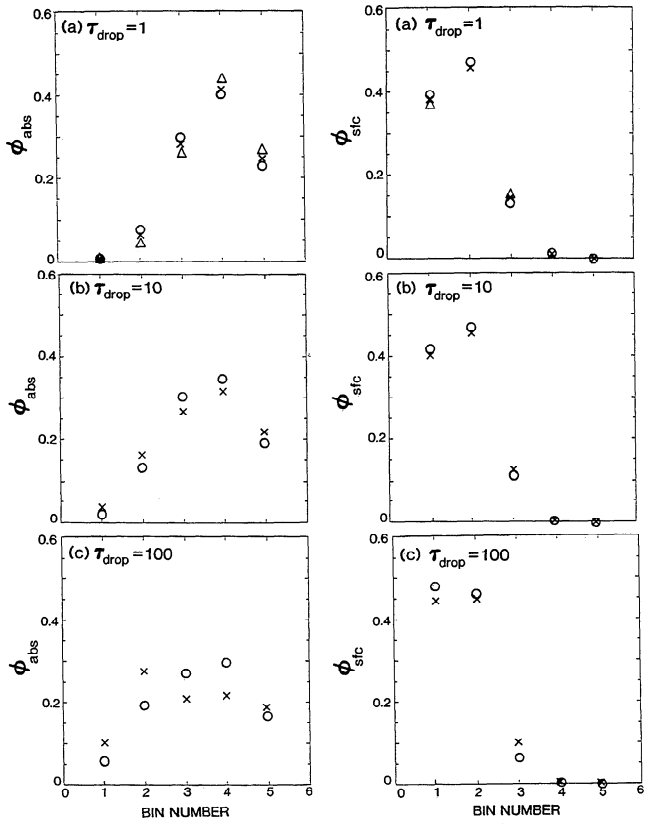

Figure 9. (Left panels) Fractional contribution (ϕ_{abs}) to the total atmospheric absorption (normalized to the total flux absorbed, S_{atm}^{abs}) in each water vapor optical depth category (see section 5). The various categories symbolize the strength of water vapor absorption over 1 cm^{-1} intervals as follows: 1, very weak; 2, weak; 3, moderate; 4, strong; and 5, very strong. The spectral results for the overcast sky cases are grouped into one of the five appropriate categories. Clear-sky (triangles) and high (crosses) and low (circles) CS cloud cases with drop optical depths of (a) 1, (b) 10, and (c) 100 are considered. Solar zenith angle is 3°. (Right panels) Same as the left panels except plotted for the fractional contribution (ϕ_{sfc}) to the total transmission at the surface ($S_{sfc}^{\downarrow}$).

arriving at the surface principally in the weakly absorbing (but nonzero absorption) vapor bands. Because of the transparency of the atmosphere with respect to vapor in these bands, the altitude of location of drops does not matter. Because of the decoupling from the vertical location of the cloud, the spectral surface flux is thus dependent primarily on the drop optical depth, in drastic contrast to the atmospheric absorption which depends critically on the vapor and cloud height. The result here necessarily demands that the dependence of the near-infrared surface flux on drop optical depth follows a functional form that is independent of cloud height, as illustrated in Figure 2c for CS clouds.

It is important to note that a substantial portion of the atmospheric absorption in clear and overcast skies occurs in bands that are not completely saturated (vapor optical depths 0.1–1) and that a small portion of the surface flux occurs in bands that are not completely transparent (vapor optical depths 0.1–1). Thus in a quantitatively rigorous sense, it is inappropriate to consider the near-infrared water vapor spectrum as being totally saturated or totally transparent. Instead, the reality is in between the two idealizations, with the near- to fully saturated regions accounting for considerable atmospheric absorption and the near-transparent regions for most of the surface flux.

On the basis of sections 4 and 5, for each cm^{-1} interval as well as any combinations of them right up to the total flux in the near-infrared spectrum, an algebraic expression can be formulated which relates the differences in the TOA-reflected and atmospheric-absorbed fluxes between two clouds located at altitudes A and B and having the same drop-size distribution:

$$-\delta\sigma_{TOA}^{\uparrow}\,[\text{cloud A} - \text{cloud B}] \sim \delta\sigma_{abs}^{atm}\,[\text{cloud A} - \text{cloud B}].$$

Figure 10 illustrates the approximate validity of the above relationship by differencing the spectral flux results for the high- and middle-cloud cases (τ_{drop} = 10). A slight offset from an exact equivalence is seen (more for (high-low)) because the difference in reflection in any interval is actually slightly less in magnitude than that in atmospheric absorption. Consequently, the surface flux difference between clouds at different levels is not identically zero; however, the departures from zero are seen to be quite small (<5 W/m^2) for the entire drop optical depth range considered in this study.

6. Cloud Forcing

We now consider other parameters that potentially play an important role in governing the solar flux disposition in overcast atmospheres. We pursue this portion of the sensitivity study by expressing the results in terms of "cloud forcing," i.e., the flux difference between the cloud and the clear-sky cases. We consider now both CS and CL clouds.

The left and right panels of Figure 11 illustrate the spectral forcing of the atmospheric absorption and that at the surface,

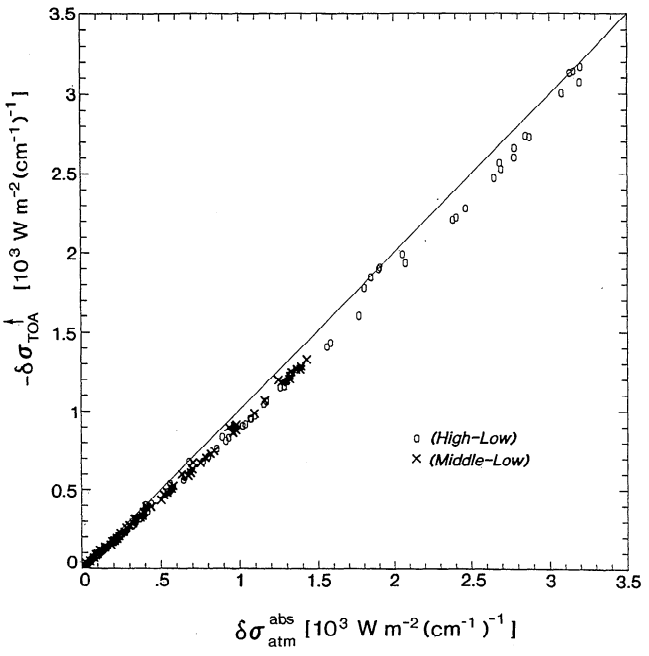

Figure 10. Difference in spectral reflection plotted against that in absorption between high and low CS clouds and between middle and low CS clouds (drop optical depth is 10). The solid line depicts the situation when the two quantities would balance each other perfectly. Solar zenith angle is 3°.

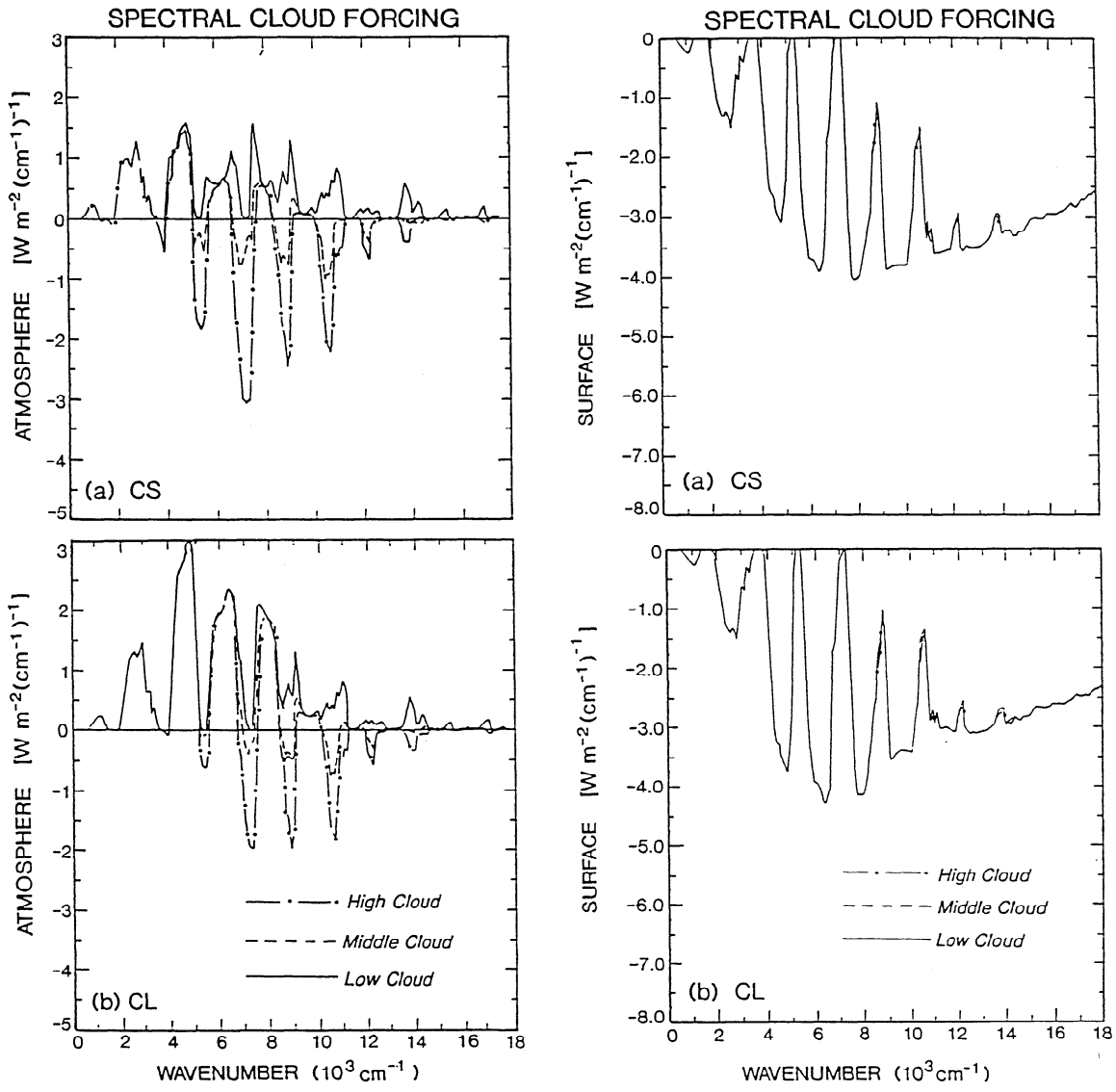

Figure 11. (Left panels) Spectral forcing of atmospheric absorption for (a) CS and (b) CL high, middle, and low clouds (drop optical depth is 10). Solar zenith angle is 3°. (Right panels) Same as the left panels except for the flux reaching the surface.

respectively, by CS and CL high-, middle-, and low-cloud placements (τ_{drop} = 10; solar zenith angle = 3°). Compared to CS, the larger drop size of CL, and hence a larger single-scattering coalbedo (Figure 1c), results in a relatively greater spectral absorption. The low CS cloud yields the same or higher atmospheric absorption than the clear sky in nearly all intervals, but this is not so for the middle and high clouds, which, in various spectral regions, can absorb less or more than clear sky. The low CL cloud yields a spectral absorption that also exceeds clear sky. By virtue of larger drops, the middle- and high-level CL clouds can have a positive forcing in spectral regions where the corresponding CS cloud exhibits a negative forcing. Below 5000 cm^{-1} there is no significant dependence on location for either CS or CL. The spectral surface forcing for CS (or CL) clouds at any location (Figure 11b) is approximately similar, with a reduction from the clear-sky flux values. As with CS, the surface flux for CL is insensitive to the cloud vertical placement.

The total near-infrared cloud forcing of the atmosphere and surface as a function of drop optical depth is shown in Figures 12 and 13, respectively. The dependence of atmospheric absorption on cloud location is quantitatively different for CS and CL clouds. With increasing drop optical depth the absorption by the CL cloud increases relatively more rapidly than for CS. The larger drop size, in fact, leads to a positive forcing for the high CL cloud in contrast to the CS result. Further, in the case of the middle cloud, there is an increase in absorption with optical depth for the CL type, in contrast to the negligible variation for CS (see also Figure 2b). The bottom panel of Figure 12 illustrates the differences between the two cloud models. The differences in cloud forcing between CS and CL are substantial and increase with optical depth. This is more so for high clouds, with the above-cloud vapor's role damping somewhat the differences for the middle- and low-cloud placements.

Figure 13 illustrates the near invariance of the total surface flux for both CS and CL clouds with respect to cloud location and for all drop optical depths. Note that the surface flux

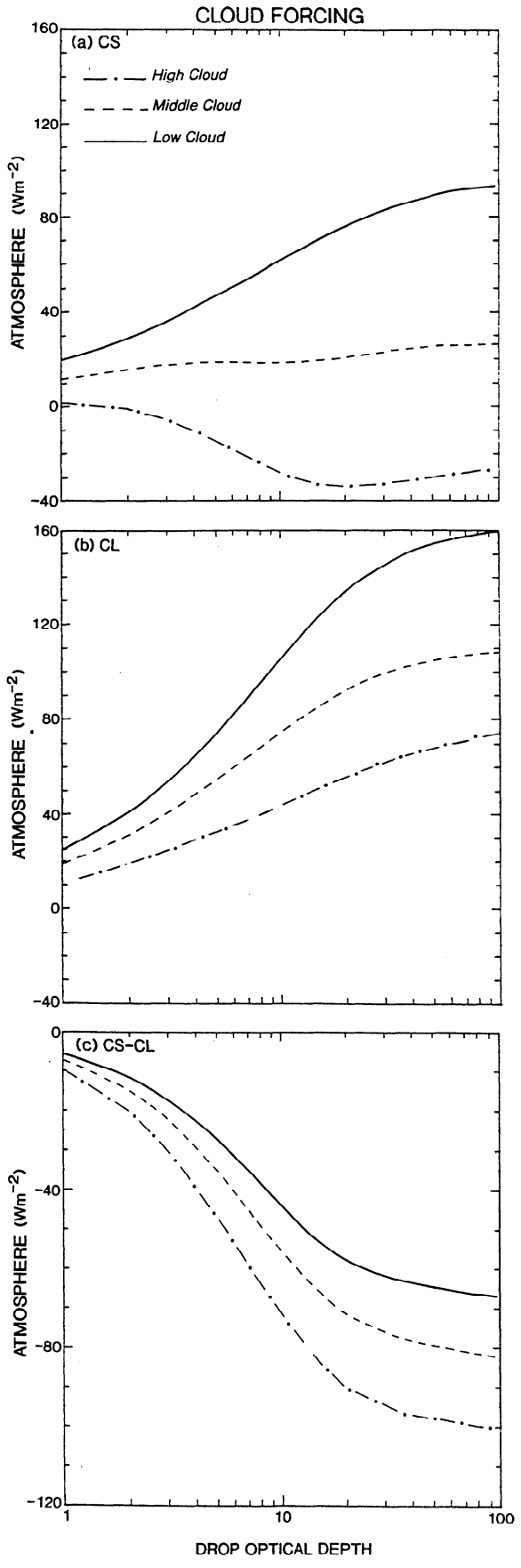

Figure 12. Atmospheric absorbed flux as a function of drop optical depth for CS (top), and CL (middle) high, middle, and low clouds. Bottom panel presents the (CS-CL) values.

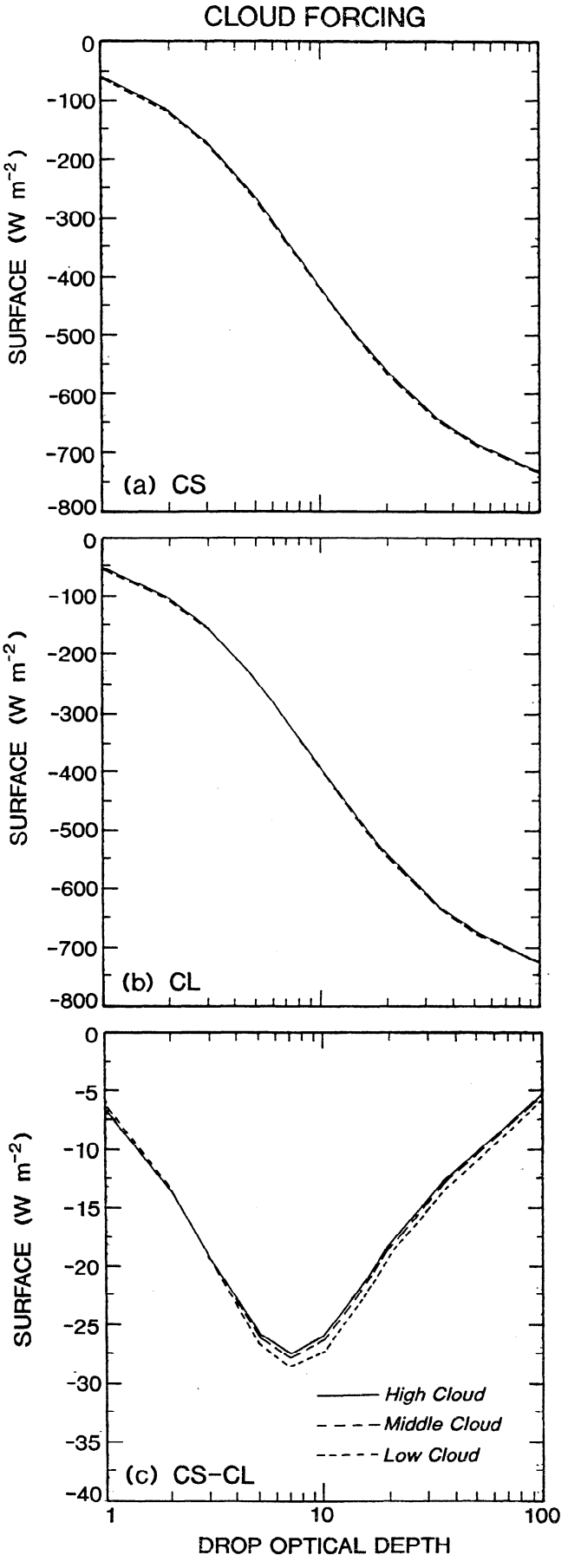

Figure 13. Same as Figure 12 except for the flux reaching the surface.

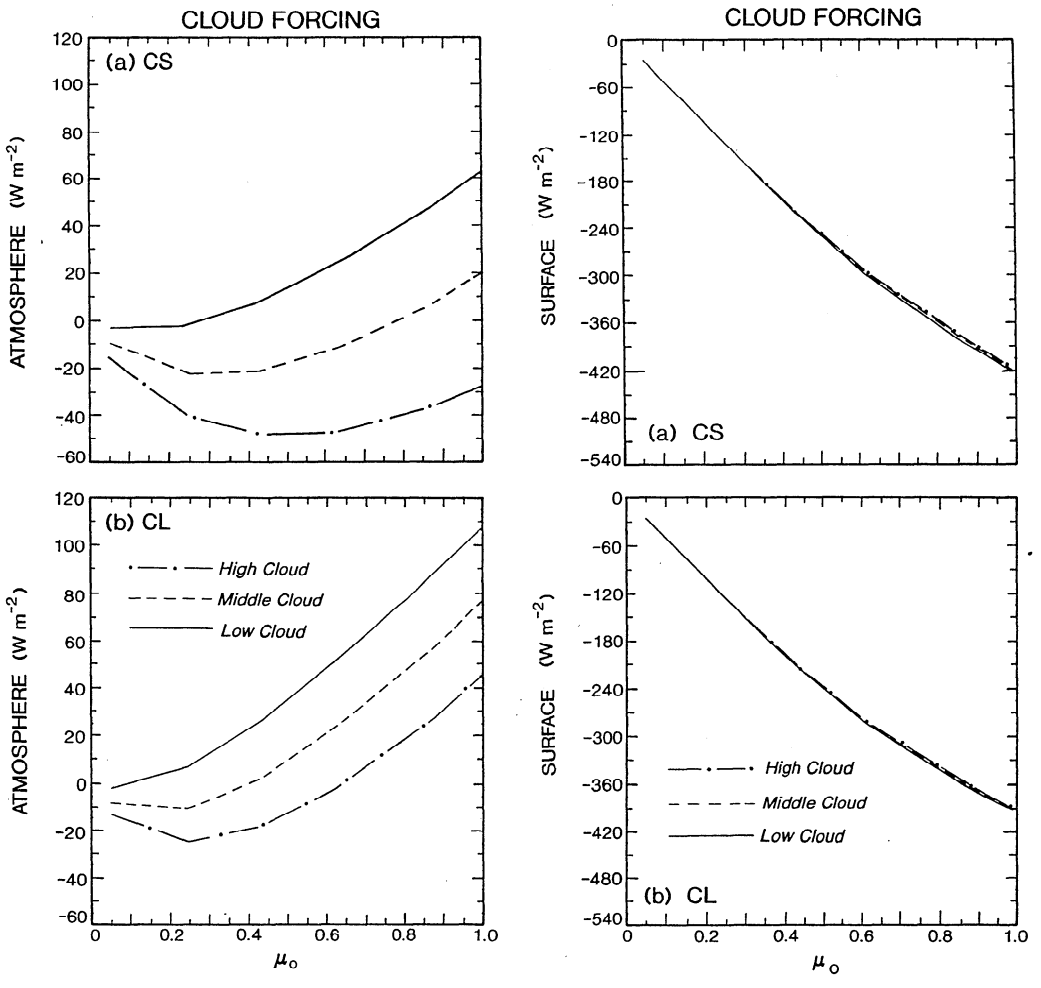

Figure 14. (Left panels) Cloud forcing of atmospheric absorption as a function of the cosine of the solar zenith angle for high, middle, and low (a) CS and (b) CL clouds (drop optical depth is 10). (Right panels) Same as the left panels except for the flux reaching the surface.

forcing for cloudy atmospheres is the least at low optical depths and most at high ones, in contrast to the feature for the fluxes (Figure 2c). The differences between CS and CL clouds are relatively small, with the maximum absolute difference being 28 W/m^2 at $\tau_{drop} \cong 7$. Figure 13 implies that surface flux changes relatively less due to drop size provided the optical depth is held constant; this is to be contrasted with the differences in their atmospheric absorption (Figure 12). Combining Figures 12 and 13, it is noted that just as for CS (Figure 2) the high CL cloud reflects more than the low one.

Figure 14 illustrates the variation of the total near-infrared atmospheric absorption (left panels) and surface (right panels) forcing with respect to the cosine of the solar zenith angle (μ_0) for $\tau_{drop} = 10$. Again, the larger drop-size of CL results in greater absorption than CS. This causes the change in the sign of the forcing from a negative to a positive value to occur at a lower μ_0 (higher solar zenith angle) for CL relative to CS. Figure 14 demonstrates that for any solar zenith angle, there is a constancy of the total surface flux with respect to cloud location.

Analyses of the spectral results (not shown) indicate that there is a near invariance of the surface flux in all the frequency intervals (as in Figure 6). For both cloud types and for all solar incident angles, the discussions concerning Figure 9 (section 5) are seen to hold true.

7. Sensitivity to Cloud Geometrical Thickness

We inquire next into the sensitivity of the results when clouds of different geometrical thicknesses are considered. The effect of increasing cloud geometrical thickness increases the amount of saturated water vapor amount within the cloud and thus the cloud layer's single-scattering coalbedo. A sensitivity study is carried out by performing computations for different CS clouds, with the cloud base pegged at 900 mbar, while cloud top height is varied but with all cases having the same drop optical depth ($\tau_{drop} = 10$) under 3° Sun conditions. Figure 15a illustrates that the amplitude of the spectral absorption can differ slightly (<0.1% of S_0) between the 800–900 mbar cloud (the nominal low cloud) and the other cases considered owing to the in-cloud vapor content differences. Throughout the spectrum and especially at wavenumbers less than ~11,000 cm^{-1}, the 180–900 mbar case reflects more radiation than the other cases (Table 2) due to less above-cloud vapor. This leads to a lesser amplitude at all of the absorption maxima locations.

The total near-infrared absorption for all cloud cases (Table 2) is a net result of the balance between reflection, interactions with the vapor above and that contained within cloud, or lack thereof. The 880–900 and 800–900 mbar clouds have a greater atmospheric absorption than the 180–900 and 300–900 mbar

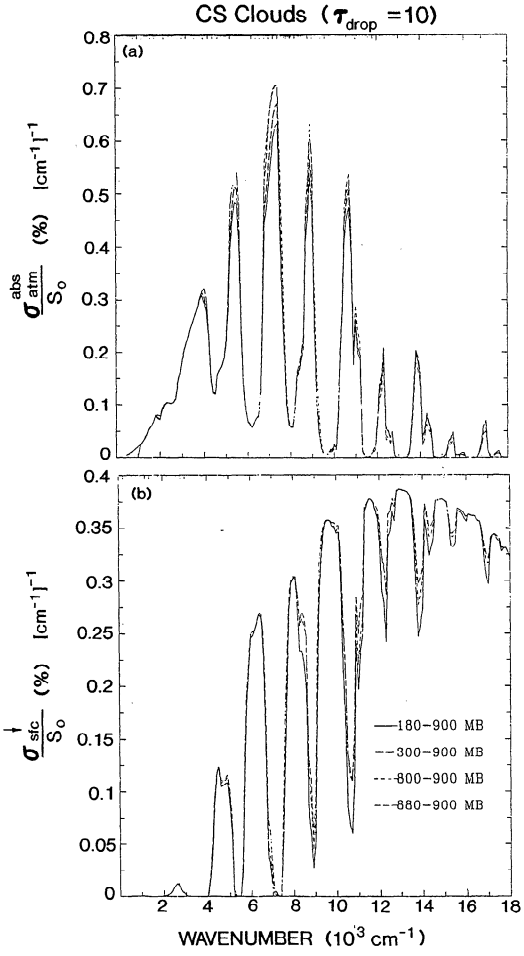

Figure 15. Spectral distribution of (a) atmospheric absorption and (b) surface flux for CS clouds (drop optical depth is 10) with cloud base at 900 mbar but with the cloud tops located at various altitudes as indicated. Solar zenith angle is 3°. The spectral flux results are expressed as a fraction of the total TOA near-infrared insolation.

cases since they allow for greater interaction of the radiation with the atmospheric water vapor and have a lesser reflecting ability. The 800–900 mbar cloud has more in-cloud vapor and thus slightly more absorption than the 880–900 mbar cloud. The 500–900 mbar case reflects more radiation than the 800–900 mbar case but also absorbs the most. The 500–900 mbar case thus represents an optimal effect of the interactions involving reflection and absorption by above- and in-cloud vapor.

Table 2. Solar Flux Absorbed in the Atmosphere, Surface Flux, and TOA-Reflected Fluxes (W/m^2) in the Case of Clouds With Different Geometric Thicknesses

Cloud Location, mbar	S_{atm}^{abs}	$S_{sfc}^{\downarrow}$	$S_{TOA}^{\uparrow}$
180–900	226.6	342.5	395.2
300–900	237.6	342.5	385.0
500–900	250.2	343.8	371.1
800–900	248.9	355.6	360.6
880–900	242.2	362.7	360.1

All have drop optical depths (τ_{drop}) of 10. The cloud base is at 900 mbar, while the cloud tops are at various altitudes as listed. Solar zenith angle is 3° (see section 7).

The near-similar reflection by the 880–900 and 800–900 clouds implies that clouds low enough in the troposphere (i.e., below a significant amount of vapor) lack a sensitivity of the albedo to their height. From Table 2 it is not possible to infer a simple relation between absorption and cloud geometric thickness, although the reflected flux generally increases with increasing cloudtop height (as in Figure 2a). The differences in the reflected and absorbed fluxes in Table 2 suggest that the earlier inferences about their anticorrelation (Figure 10) become weaker when clouds with very large geometric thicknesses are considered. Note that the difference in atmospheric absorption between the 180–900 and 800–900 mbar clouds is much less (~10% in Table 2) than that seen earlier between the 800–900 and the 180–200 mbar clouds (~36% (Figure 2b and Table 4)). This is because, in contrast to the 180–200 mbar cloud, the 180–900 mbar cloud, besides having a greater reflection, also yields a greater absorption owing to its large in-cloud vapor content.

Figure 15b illustrates the spectral distribution of the surface flux. In the weak absorption intervals the amplitudes for all cases are roughly similar. However, in regions of moderate-to-strong absorption (e.g., 7400, 8900, 10,800, 11,000, 13,600 cm^{-1}), there arise differences due to an overall increase of atmospheric water vapor content; these exceed those in Figure 6. Table 2 indicates that the surface flux is reduced monotonically as cloudtop height, and thus in-cloud vapor, is increased. The surface flux exhibits a slightly larger variance than in the cases discussed earlier (differences relative to the 800–900 mbar case are <4% compared to ~1.5% in Figure 2c; see also Table 4). This tempers slightly the near-invariance feature of the surface flux to cloud location for extensive clouds.

8. Sensitivity to Atmospheric Profile

While all of the preceding sensitivity analyses employed the MLS atmospheric profile, we consider next the effects in atmospheric conditions with different moisture profiles. Specifically, we consider the tropics (T) and subarctic winter (SAW) profiles of *McClatchey et al.* [1972]. Table 3 lists the total amount of water vapor and the clear-sky absorbed flux for 3° Sun conditions (the Sun angle chosen is merely to demonstrate the differences arising due to vapor amounts). SAW holds less moisture and thus yields substantially less absorption than MLS or T. The spectral atmospheric absorbed fluxes and the differences with respect to MLS are illustrated, respectively, in Figures 16a and 16b. The amplitudes of the spectral absorption reflect the difference in moisture amounts. The difference of

Table 3. Column Water Vapor Amounts and Near-Infrared Fluxes Absorbed in the Midlatitude Summer (MLS), Tropical (T), and Subarctic Winter (SAW) Atmospheres Under Clear-Sky Conditions Containing Water Vapor Only

Atmospheric Profile	Column Vapor, kg/m^2	Atmospheric Absorption	
		W/m^2	%
MLS	29.3	187.1	19.4
T	41.3	205.5	21.3
SAW	4.4	102.3	10.6

Solar zenith angle is 3° and the TOA insolation is 966 W/m^2 in each case (see section 8).

SAW results from MLS is striking; the systematic spectral differences lead to a large difference in the total absorbed flux (Table 3). The effects of moisture on the spectral downward surface flux (Figure 16c) are comparable for MLS and T, but both differ substantially from SAW.

The differences in the moisture profiles have the potential to affect the magnitude of absorption occurring above clouds. An additional point to consider is that the assumption of saturation within clouds in the warmer profiles (MLS and T) would lead to even greater moisture content differences with respect to SAW. Thus it is important to determine whether the surface flux in SAW and T exhibit tendencies analogous to MLS for similar cloud types and vertical placements. Table 4 lists the values of atmospheric absorbed and surface fluxes (3° Sun conditions) for low- and high-cloud locations (CS cloud; $\tau_{drop} = 10$). The actual surface flux is substantially different for each profile under similar cloud conditions, being largest for the drier SAW profile. However, the surface flux remains nearly invariant (to ~1.5%) with respect to cloud location for a fixed drop optical depth in both the SAW and the T profiles, albeit with a different magnitude than in MLS. As in MLS, the atmospheric absorption for high- and low-cloud cases differ substantially, with SAW having the least difference by virtue of its more transparent atmosphere. For high clouds, when the above-cloud vapor effect is the least, the results for the reflected flux are approximately similar for the various profiles. For all profiles the difference between the high- and the low-cloud atmospheric absorption matches approximately (to within ~5 W/m^2) the corresponding changes in their reflection, consistent with section 5.

9. Relation Between Surface and TOA Fluxes

The discussions in sections 3–5 bear on an important practical issue regarding clear and overcast skies, namely, the relationship between the TOA and the surface fluxes. Here we explore the relationships between these parameters based on the present computations. An important motivation for doing so is the need to deduce simple relationships on a firm theoretical basis, such that satellite-measured TOA fluxes may be used to retrieve the net surface flux [e.g., *Schmetz*, 1993].

Considering first water vapor alone, LBL computations are performed for different solar incident angles, which is tantamount to considering different optical pathlengths through the MLS atmosphere. The relationship of the net flux at the surface to that at the top for the different Sun angles is illustrated in Figure 17. For a given surface albedo, there results a simple linear dependence, implying that the inference of near-infrared net ($\downarrow - \uparrow$) surface solar flux from net ($\downarrow - \uparrow$) TOA flux has a firm theoretical basis. However, the slope does depend on the value of the surface albedo. The linearity is merely an expression of the simple scaling of the water vapor absorption with respect to the zenith angle of the beam [e.g., *Schmetz*, 1993]. As TOA flux gets smaller at large solar zenith angles,

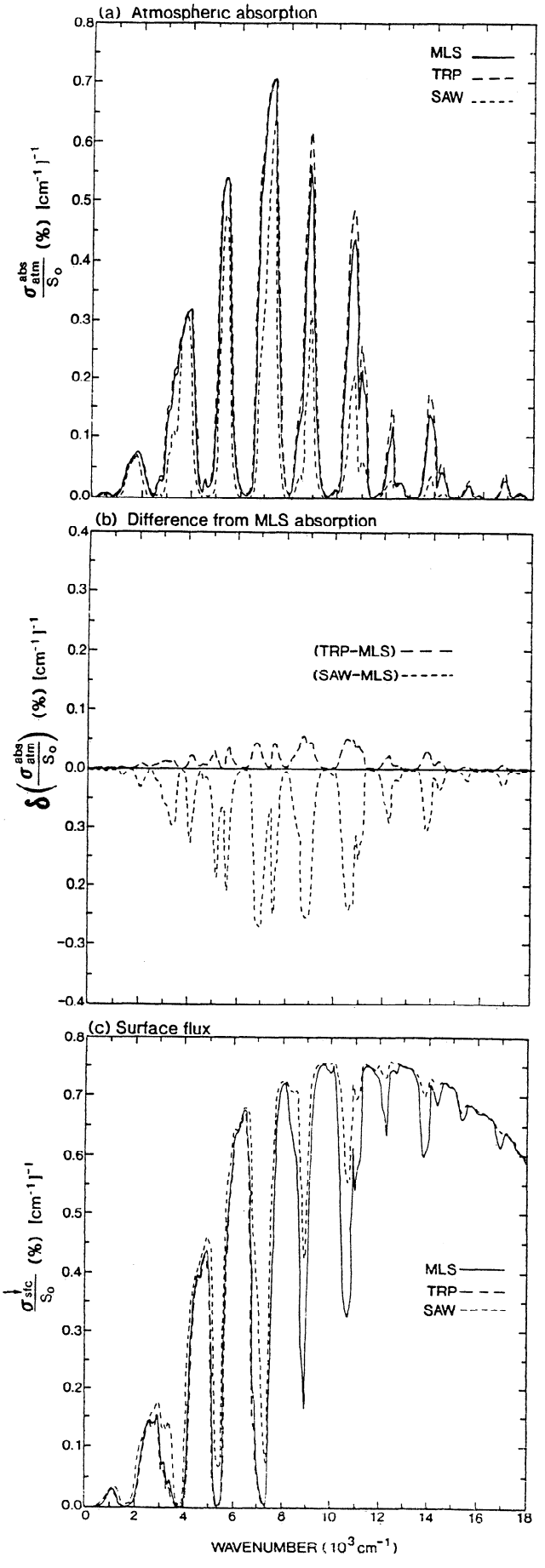

Figure 16. Spectral flux distribution in clear skies containing water vapor, obtained by using three different atmospheric profiles (MLS, SAW, and T). (a) Flux absorbed in the atmosphere, (b) difference in the atmospheric absorption from the MLS values, and (c) the surface flux. Solar zenith angle is 3°. The spectral flux results are expressed as a fraction of the total TOA near-infrared insolation.

Table 4. Solar Flux Absorbed in the Atmosphere and the Surface Flux for CS Type Cloud in Different Atmospheres (MLS, T, and SAW)

Profile	Cloud	Atmospheric Absorption, W/m^2	Surface Flux, W/m^2	Reflected Flux, W/m^2
MLS	high	158.9	361.2	445.0
	low	248.9	355.6	360.6
T	high	168.1	352.1	444.8
	low	266.0	347.2	352.0
SAW	high	121.5	398.4	445.2
	low	169.7	396.8	398.6

All have drop optical depths (τ_{drop}) of 10, with the cloud located either in the 800–900 mbar (low) or the 180–200 mbar (high) layers. Solar zenith angle is 3° (see section 8).

Table 5. Least Squares Linear Fit Between the Net (= (Down − Up)) TOA and Surface Near-Infrared Fluxes (W/m^2) for Clear-Sky MLS Conditions Corresponding to the Plot Shown in Figure 17

Surface Albedo	Linear Fit
0	$S_{sfc}^{net} = -17.55 + 0.81\, S_{TOA}^{net}$
0.8	$S_{sfc}^{net} = -6.94 + 0.41\, S_{TOA}^{net}$

Two different Lambertian surfaces are considered. The relations are valid for surface fluxes greater than 0 (see section 9).

the optical path length becomes increasingly large such that very little radiation reaches the surface; in fact, the values at extremely large zenith angles differ slightly from the slope constructed using mainly the smaller zenith angles. Table 5 lists the linear fit obtained for surface albedos of 0 and 0.8, respectively; these are comparable to *Schmetz* [1993].

From the previous sections the surface flux is mainly a function of drop optical depth, provided the atmosphere contains a nominal amount of water vapor. In contrast, the atmospheric absorption is a strong function of the cloud location, which acts to counter the changes in reflection. Thus with respect to differences in cloud height, the near-infrared TOA (i.e., surface plus atmosphere system) and surface fluxes cannot be linked unambiguously since the former varies with location while the latter does not. We demonstrate the consequence of this point in Figure 18 for CS and CL clouds (3° Sun angle). Each horizontal trio of points represents a particular drop optical depth (τ_{drop} varying from 1 to 100), while the individual points for each trio comprise solutions, respectively, for the low, middle, and high clouds.

Near the top right-hand portion of the plot, the results for the different cloud heights are relatively less distinguishable

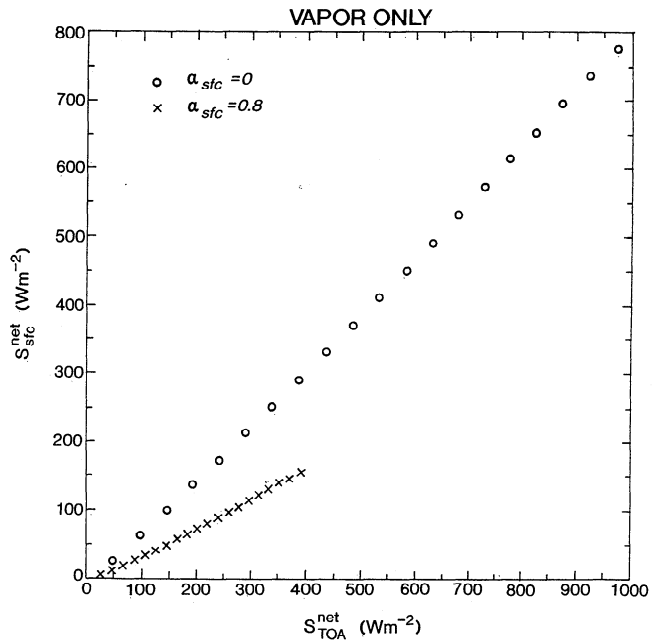

Figure 17. Scatterplot of the results for the net surface flux versus the net TOA flux for clear-sky conditions. The different points represent computations at different solar angles of incidence. Two different surface albedos (0 and 0.8) are considered.

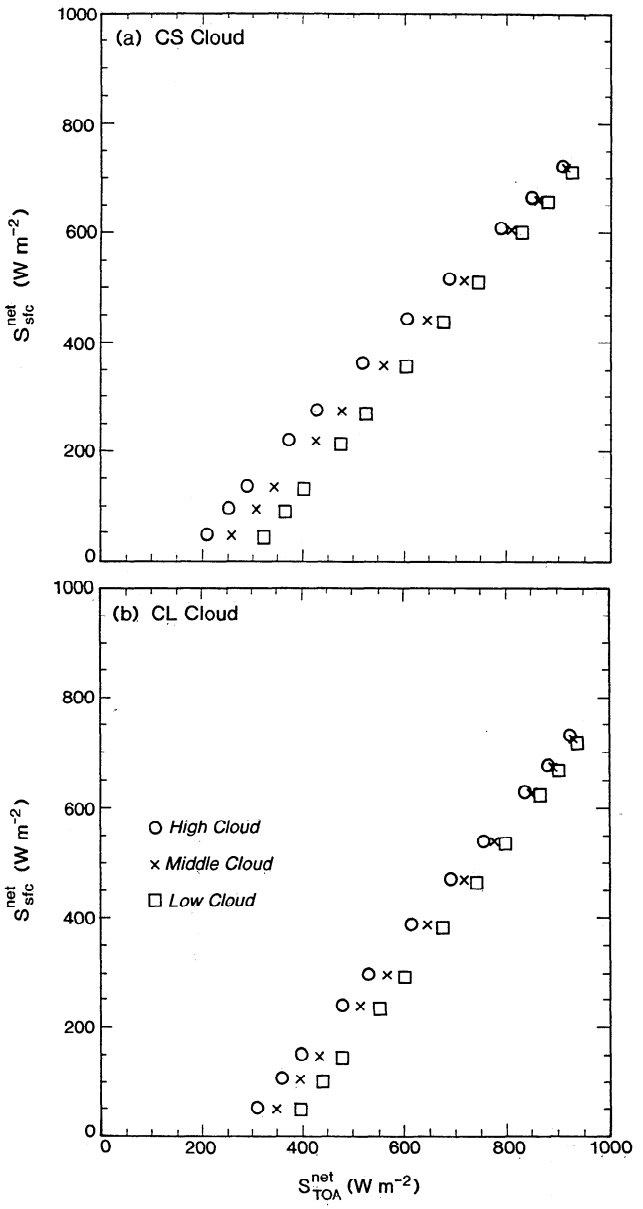

Figure 18. Scatterplot of the results for the net surface flux versus the net TOA flux for (a) CS and (b) CL clouds. Different optical depths and high-, middle-, and low-cloud locations are considered. Solar zenith angle is 3°.

since drop optical depth is too small for the location to be an important factor (compare Figure 2 and 4). Toward the progression to the bottom left-hand corner of the plot, the larger τ_{drop} values result in an increasing difference in the TOA flux between high and low clouds, with the surface flux being relatively invariant (compare Figures 2, 4, and 13). Both CS and CL clouds exhibit a similar pattern, with the CL case having a lesser reflection (by virtue of a greater coalbedo and a greater asymmetry factor) for a given τ_{drop} than the corresponding CS case (compare Figures 1b, 1c, and 12).

Thus under the conditions assumed, the sensitivity to cloud location and to some extent the drop-size distribution inhibits the derivation of a simple general relationship between the TOA and the surface fluxes, in contrast to the clear-sky situation in Figure 17. However, while all three cloud heights do not yield a linear relationship when considered together, for any specific cloud location, it is possible to associate the TOA and surface flux parameters in a linear manner (see best fit relations listed in Table 6). The differing functional dependence on drop optical depth for the clouds at the three altitudes and the two drop distributions are manifest in the derived slope values. The maximum difference in slope, using $\tau_{drop} = 10$ as a reference, is ~17% for CS and 14% for CL. For a specific cloud height the slope difference between CS and CL is <15%. Hence if cloud drop sizes for a particular cloud height are known a priori, it may be possible to infer the surface flux from the TOA flux in a simple manner. A cautionary note here is that knowledge of cloud base or, equivalently, the cloud geometrical extent is also necessary for a precise estimate (Figure 16, Table 2).

Since the amount of incident flux and drop scattering characteristics depend on the solar zenith angle, this parameter may also be expected to affect the TOA-surface relationship. While the above discussions pertain to the 3° Sun angle, similar conclusions hold when computations are performed (not shown) at other zenith angles. Again, holding cloud height fixed and considering the drop optical depth to range from 1 to 100, it is possible to obtain linear best fits to the TOA-surface relationship. As an example, Table 7 lists the relationships for the low CS cloud case at different angles. The difference in slopes ranges up to ~10%. An important inference is that for a fixed cloud placement, even though the water vapor amount above the cloud alone can probably be factored in simply (as Figure 17 implies) leading to a simple TOA-surface relationship, drops introduce a zenith-angle dependent complication into the relationship, consistent with *Schmetz* [1993].

Table 6. Least Squares Linear Fit Between the Net (= (Down − Up)) TOA and Surface Near-Infrared Fluxes (W/m^2) for CS and CL Clouds Corresponding to Plots Shown in Figure 18

Cloud	Altitude	Linear Fit
CS	high	$S_{sfc}^{net} = -144.76 + 0.96\ S_{TOA}^{net}$
	middle	$S_{sfc}^{net} = -217.28 + 1.02\ S_{TOA}^{net}$
	low	$S_{sfc}^{net} = -322.48 + 1.12\ S_{TOA}^{net}$
CL	high	$S_{sfc}^{net} = -293.39 + 1.10\ S_{TOA}^{net}$
	middle	$S_{sfc}^{net} = -355.90 + 1.15\ S_{TOA}^{net}$
	low	$S_{sfc}^{net} = -454.64 + 1.25\ S_{TOA}^{net}$

Optical depths considered range from 1 to 100. Low, middle and high cloud locations are considered for solar zenith angle of 3 degrees. The relations are valid for surface fluxes greater than 0. (See Section 9).

Table 7. Same As Table 6 Except for the 800–900 mbar (Low) Cloud Location and Various Solar Incidences

Solar Zenith Angle	Linear Fit
75	$S_{sfc}^{net} = -67.76 + 1.02\ S_{TOA}^{net}$
65	$S_{sfc}^{net} = -117.81 + 1.04\ S_{TOA}^{net}$
52	$S_{sfc}^{net} = -178.50 + 1.07\ S_{TOA}^{net}$
30	$S_{sfc}^{net} = -268.61 + 1.10\ S_{TOA}^{net}$
3	$S_{sfc}^{net} = -322.48 + 1.12\ S_{TOA}^{net}$

See section 9.

10. Discussions

High spectral resolution computations of the near-infrared solar radiation interactions in overcast atmospheres reveal the distinct signature of water vapor on the fluxes and its modulation of the drop effects. This modulation, however, becomes less pronounced for high clouds and can even be suppressed when these clouds have large drop optical depths. Consistent with earlier studies [e.g., *Liou*, 1976; *Stephens*, 1978; *Davies et al.*, 1984; *Wiscombe et al.*, 1984; RF92], the atmospheric absorption is strongly determined by the amount of vapor that the solar beam traverses before reaching cloud top. Thus low clouds yield a higher atmospheric absorption for the same drop optical depth than high clouds, with the cloud, atmosphere, and atmosphere plus surface absorption exhibiting different sensitivities to drop optical depths at the various altitudes. The flux absorbed within clouds is maximized for optically thick high clouds, while the flux absorbed by vapor above low clouds and below high clouds can be as significant as that absorbed within clouds.

Because of the role of water vapor the difference in the forcing of atmospheric absorption between high and low clouds increases with drop optical depth [cf. *Schmetz*, 1993]. The above-cloud vapor absorption leads to a positive forcing of the atmospheric absorption for lower-troposphere clouds (i.e., greater absorption than clear sky). Clouds with the same optical depth but consisting of larger drops at any altitude yield more absorption than those with smaller radii. Thus high clouds comprised of large particles can actually yield a positive instead of a negative forcing of the atmospheric absorption. The spectrally absorbed flux (or forcing) pattern (i.e., locations of peaks and troughs) is similar for different cloud heights, thicknesses, drop sizes, atmospheric profiles, and zenith angles, but the amplitudes can be strongly dependent on these variables.

In contrast, the surface flux is approximately invariant with respect to the vertical location of the cloud, not just for the total flux but also in every spectral interval, being governed principally by the drop optical depth. The behavior of the total flux is consistent with the calculations of *Chou* [1989] and *Schmetz* [1993]. Although the actual magnitude of the surface flux differs for various solar angles, atmospheric profiles (ranging from warm, moist to cold, dry conditions), and cloud geometrical thicknesses (containing different saturated water vapor amounts), its variance with the altitude placement of the cloud for fixed drop optical depth, as estimated from the results in this study, is less than ~6%. Also, with other parameters remaining the same, the surface flux differs by less than 10% (absolute differences <25 W/m^2) for the two drop distributions considered here. This degree of invariance does not

exist for the atmospheric absorption with respect to changes in any of the above mentioned variables.

The fundamental causes of the near invariance of the spectral and total surface fluxes with respect to cloud height are (1) in the moderate to strongly absorbing vapor bands (vapor optical depths of 0.1 to 10 and more), radiation is absorbed or reflected by clouds which is (or would be) otherwise absorbed by water vapor and thus fails to reach the surface; it is to be noted that even in clear skies the surface flux is quite small in such absorption bands; and (2) ~85% or more of the solar flux that does reach the surface in clear or overcast skies is confined to spectral regions where water vapor does not absorb strongly (vapor optical depths <0.1); in such bands, the atmosphere is nearly transparent as far as vapor is concerned, the interaction becomes governed entirely by drops (consisting of reflection, transmission, and absorption), and thus there is little dependence on cloud location.

Because of the effects of the weak to moderately absorbing bands, the total near-infrared surface flux cannot be interpreted as symbolizing either completely saturated or unsaturated bands. The results here suggest that water vapor in the present atmosphere is of such an amount that it enables the saturation of the radiation in the "center" of the absorption bands, even for the relatively dry, subarctic atmosphere. However, it is not enough to prevent radiation in the weak bands from reaching the surface. The high spectral resolution results here strongly corroborate the results of *Schmetz* [1993] and demonstrate and explain the near-invariance feature of the near-infrared spectral surface flux. It would appear that for a particular drop-size distribution, one can expect the surface flux in overcast skies to be governed mainly by the drop optical characteristics. The results also reiterate that water vapor absorption and its nonmonotonic spectral variation must be carefully accounted for, particularly when moderately absorbing frequencies and low clouds are considered. This is especially important for solar surface flux computations since their magnitude affects critically the surface heat and water balance [e.g., *Chen and Ramaswamy*, 1995] (note that WCRP requirements are that the monthly mean biases be less than ~10 W/m^2).

The difference in reflection over any spectral interval and, consequently, the entire spectrum, between columns containing clouds at different altitudes (all having the same drop optical depth) is approximately the negative of the corresponding differences in the atmospheric absorption. Thus if there are no large variations in drop sizes and optical depths with altitude, any change in reflection for different overcast situations over oceans, as measured at TOA by satellites, would imply a change of opposite sign in the atmospheric absorption, irrespective of the cloud vertical location. At the very least, this should be valid for water clouds (say, located at ~500 mbar and below). Simultaneous measurements of optical depth and near-infrared fluxes could allow a test of this theoretically derived feature. While the spectral surface flux in the water vapor "windows" can be retrieved from spectral TOA measurements (because of insensitivity to water vapor), this cannot be extrapolated to obtain the total spectrum flux (H97).

The results here indicate that for overcast atmospheres in general, the TOA fluxes cannot yield unambiguous information about the surface or atmospheric absorbed fluxes without additional knowledge of the cloudtop height, geometrical thickness, drop optical depth, and the amount of water vapor above and inside clouds. Atmospheric absorption is not an invariant quantity, and the TOA flux is decoupled from the surface flux throughout the spectrum. This places earlier inferences obtained for total fluxes using coarser spectral resolution and/or lower-order multiple-scattering methods on a much more firm footing. The behavior for overcast atmospheres is in contrast to the case with water vapor only when a linear relation between TOA and surface fluxes becomes possible, with only an added dependence on surface albedo that can be accounted for simply. Thus the linear relationships sometimes assumed between cloudy sky TOA and surface fluxes [see *Schmetz*, 1993 for discussions], independent of cloud height and the geometrical and optical depth, have to be treated with considerable caution as they are not prevalent in general but require certain conditions, such as clouds at a fixed height and Sun angle (when the role of above-cloud vapor is fixed). The significance of cloud height and Sun angle have been emphatically recognized [*Chou et al.*, 1995; *Masuda et al.*, 1995]. Although errors may be unavoidable in the absence of any other method to infer the surface fluxes, there cannot be a high degree of confidence in applying specific TOA-surface flux relationships universally.

This study has considered only two somewhat different water drop-size distributions. One extension to the study here would be a similar pursuit incorporating ice crystal optical properties at the high altitudes. The results here are based on plane-parallel theory and the presently known spectral parameters of water vapor. It is unlikely that uncertainties in water vapor absorption and cloud optics, or the inclusion of other constituents (e.g., other molecular species, aerosols) will alter the general conclusions of this study, namely, near independence of the surface flux from and the critical dependence of atmospheric absorption on the vertical cloud placement. This study has used a "zero" surface albedo and the inferences hence are applicable primarily to oceanic regions.

The results here, together with earlier ones, present an intriguing picture of the strong correlation of the near-infrared surface fluxes with hydrometeor properties and its decoupling from the atmospheric absorption for a wide range of parameter values. It must be noted that the surface flux feature deduced here has been for drop optical depths of 1 or more. For particulate optical depths smaller than 1 (e.g., thin haze layer), this may not necessarily hold in view of the potential influence of Rayleigh scattering.

The feature obtained here could be confirmed (or refuted) by making measurements of drop optical depth and water vapor amount coincident with spectral irradiance measurements. If the theoretical computations are borne out by carefully conducted observations in the field, then there arises the tantalizing prospect of estimating, to a fair degree of accuracy, the global ocean surface solar flux (but not the atmospheric absorption) in skies containing water clouds from just a knowledge of the climatological vapor and prevailing drop-size distributions. If the dependence of atmospheric absorption and surface flux on cloud height and drop optical depth turns out to be different from that computed, then plane-parallel theory and the present knowledge of the water vapor spectral parameters may need to be questioned. Finite, horizontally inhomogeneous clouds pose another dilemma that needs to be investigated separately. Nevertheless, one inescapable conclusion is that if the TOA and surface fluxes cannot be linked in an unambiguous manner for plane-parallel, idealized clouds, there arise considerable doubts about the likelihood of a simple relation prevailing between them in more realistic cloud

conditions. Comparisons of the computed sensitivities against relevant observations also carry important implications for the robustness of radiative parameterizations employed in weather forecasting and climate models, since the high-resolution results presented here constitute reference computations against which such parameterizations are constructed and developed.

Acknowledgments. We thank J. Haywood and M. D. Schwarzkopf for their comments on the manuscript. We also thank Harshvardhan and W. Ridgway for their suggestions.

References

Chen, C.-T., and V. Ramaswamy, Parameterization of the solar radiative characteristics of low clouds and studies with a general circulation model, *J. Geophys. Res.*, *100*, 11,611–11,622, 1995.

Chou, M.-D., On the estimation of surface radiation using satellite data, *Theor. Appl. Climatol.*, *40*, 25–36, 1989.

Chou, M.-D., A. Arking, J. Otterman, and W. L. Ridgway, The effect of clouds on atmospheric absorption of solar radiation, *Geophys. Res. Lett.*, *22*, 1885–1888, 1995.

Crisp, D., Absorption of sunlight by water vapor in cloudy conditions: A partial explanation for the cloud absorption anomaly, *Geophys. Res. Lett.*, *24*, 571–574, 1997.

Davies, R., W. L. Ridgway, and K.-E. Kim, Spectral absorption of solar radiation in cloudy atmospheres: A 20 cm^{-1} model, *J. Atmos. Sci.*, *41*, 2126–2137, 1984.

Fouquart, Y., B. Bonnel, and V. Ramaswamy, Intercomparing shortwave radiation codes for climate studies, *J. Geophys. Res.*, *96*, 8955–8968, 1991.

Harshvardhan, R., Davies, D. A., Randall, and T. G. Corsetti, A fast radiation parameterization for atmospheric circulation models, *J. Geophys. Res.*, *92*, 1009–1016, 1987.

Hunt, G. E., and I. P. Grant, Discrete space theory of radiative transfer and its application to problems in planetary atmospheres, *J. Atmos. Sci.*, *26*, 963–972, 1969.

Liou, K.-N., On the absorption, reflection and transmission of solar radiation in cloudy atmospheres, *J. Atmos. Sci.*, *33*, 798–805, 1976.

Masuda, K., H. G. Leighton, and Z. Li, A new parameterization for the determination of solar flux absorbed at the surface from satellite measurements, *J. Clim.*, *8*, 1615–1629, 1995.

McClatchey, R. A., R. W. Fenn, J. E. A. Selby, F. E. Volz, and J. S. Garing, *Optical Properties of the Atmosphere*, *AFCRL-72-0497*, 110 pp., Air Force Cambridge Res. Lab., Hanscom Air Force Base, Bedford, Mass., 1972.

Ramaswamy, V., and S. M. Freidenreich, Solar radiative line-by-line determination of water vapor absorption and water cloud extinction in inhomogeneous atmospheres, *J. Geophys. Res.*, *96*, 9133–9157, 1991.

Ramaswamy, V., and S. M. Freidenreich, A study of broadband parameterizations of the solar radiative interactions with water vapor and water drops, *J. Geophys. Res.*, *97*, 11,487–11,512, 1992.

Ramaswamy, V., and J. Li, A line-by-line investigation of solar radiative effects in vertically inhomogeneous low clouds, *Q. J. R. Meteorol. Soc.*, *122*, 1873–1890, 1996.

Rothman, L. S., R. R. Gamache, A. Barbe, A. Goldman, J. R. Gillis, L. R. Brown, R. A. Toth, J. M. Flaud, and C. Camy-Perot, AFGL atmospheric absorption line parameter compilations: 1982 edition, *Appl. Opt.*, *22*, 2247–2256, 1983.

Schmetz, J., Relationship between solar net radiative fluxes at the top of the atmosphere and at the surface, *J. Atmos. Sci.*, *50*, 1122–1132, 1993.

Slingo, A., A GCM parameterization for the shortwave radiative properties of water clouds, *J. Atmos. Sci.*, *46*, 1419–1427, 1989.

Stephens, G. L., Radiation profiles in extended clouds, I, Theory, *J. Atmos. Sci.*, *35*, 2111–2122, 1978.

Wiscombe, W. J., R. M. Welch, and W. D. Hall, The effects of very large drops on cloud absorption, I, Parcel models, *J. Atmos. Sci.*, *41*, 1336–1355, 1984.

S. M. Freidenreich and V. Ramaswamy, NOAA GFDL, P. O. Box 308, Princeton, NJ 08542. (e-mail: vr@gfdl.gov)

(Received December 4, 1997; revised May 18, 1998; accepted May 27, 1998.)